Exoplanet searches with microlensing

- **А.Ф.Захаров (Alexander F. Zakharov)**
- ***Institute of Theoretical and Experimental Physics,***
- ***B. Cheremushkinskaya, 25, 117218 Moscow,***
- ***&***
- ***Boboliubov Laboratory of Theoretical Physics,***
- ***Joint Institute for Nuclear Research , Dubna, Russia***

- **Based on joint work done with G. Ingrosso (Lecce), De Paolis (Lecce), P. Jetzer (Zurich), S. Calchi Novati (Salerno), A.A. Nucita (Madrid)** (MNRAS, arXiv:0906.1050)

- **The first workshop: astrophysical winds and disks**
- **Similar phenomena in stars and quasars**
- **Platamonas, Greece,**
  September 3-8, 2009

- Reference
- New Astronomy Reviews (2009, in press)

ASTREV 1385
22 August 2009

ARTICLE IN PRESS

No. of Pages 7, Model 5G

New Astronomy Reviews xxx (2009) xxx–xxx

Contents lists available at ScienceDirect

New Astronomy Reviews

journal homepage: www.elsevier.com/locate/newastrev

Gravitational lensing: From micro to nano

Alexander F. Zakharov

Institute of Theoretical and Experimental Physics, B. Cheremushkinskaya, 25, 117259 Moscow, Russia
Bogoliubov Laboratory for Theoretical Physics, JINR, 141980 Dubna, Russia

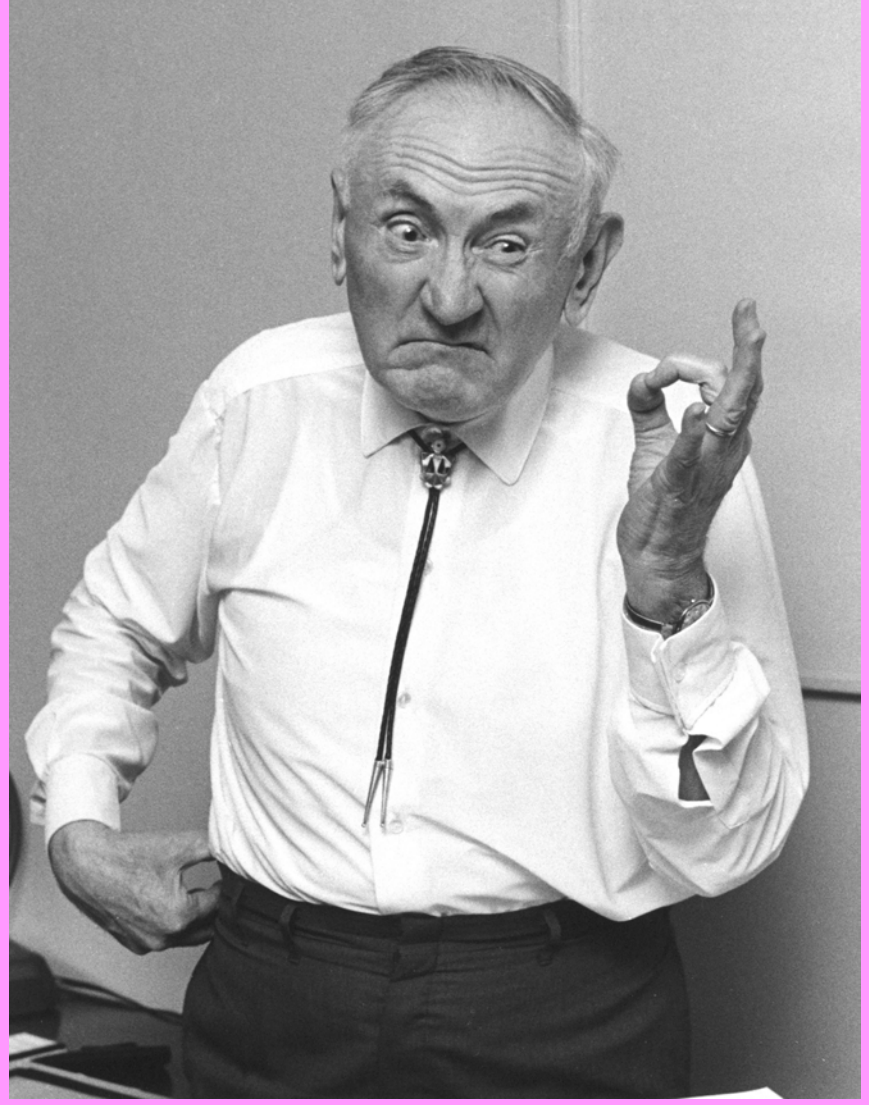

- Fritz Zwicky → DM

aber, wie man sich leicht überzeugt, auf der erwähnten Annahme beruhen.

Damit haben wir die Untersuchung des Meridianinstruments abgeschlossen. Die Untersuchung der Winkelmessung in den zur Meridianebene normalen Ebenen bringt, wie man sich leicht überzeugt, keine neuen Resultate.

Zusammenfassend können wir also sagen: der Winkelmessung liegt die Annahme der euklidischen Kinematik des starren Körpers zu Grunde. Die Verwendung optischer Hilfsapparate (Fernrohr, Mikroskop usw.) bringt keine neuen optischen Annahmen mit sich. Die »Starrheit« der Instrumente wird mit Hilfe unserer Annahme 2 und der Unabhängigkeit der Abbildungsgesetze von der Richtung geprüft. Diese letztere ist zwar noch nicht unmittelbar überprüft, kann aber durch den Ausfall des *Michelson*schen Versuches gestützt werden.

Wien, 1924 Febr. 15. *Fr. Zerner.*

Über eine mögliche Form fiktiver Doppelsterne. Von *O. Chwolson.*

Es ist gegenwärtig wohl als höchst wahrscheinlich anzunehmen, daß ein Lichtstrahl, der in der Nähe der Oberfläche eines Sternes vorbeigeht, eine Ablenkung erfährt. Ist γ diese Ablenkung und γ_0 der Maximumwert an der Oberfläche, so ist $\gamma_0 \geqq \gamma \geqq 0$. Die Größe des Winkels ist bei der Sonne $\gamma_0 = 1''.7$; es dürften aber wohl Sterne existieren, bei denen γ_0 gleich mehreren Bogensekunden ist; vielleicht auch noch mehr. Es sei A ein großer Stern (Gigant), T die Erde, B ein entfernter Stern; die Winkeldistanz zwischen A und B, von T aus gesehen, sei α, und der Winkel zwischen A und T, von B aus gesehen, sei β. Es ist dann

$$\gamma = \alpha + \beta .$$

Ist B sehr weit entfernt, so ist annähernd $\gamma = \alpha$. Es kann also α gleich mehreren Bogensekunden sein, und der Maximumwert von α wäre etwa gleich γ_0. Man sieht den Stern B von der Erde aus an zwei Stellen: direkt in der Richtung TB und außerdem nahe der Oberfläche von A, analog einem Spiegelbild. Haben wir mehrere Sterne B, C, D, so würden die Spiegelbilder umgekehrt gelegen sein wie in einem gewöhnlichen Spiegel, nämlich in der Reihenfolge D, C, B, wenn von A aus gerechnet wird (D wäre am nächsten zu A).

Der Stern A würde als fiktiver Doppelstern erscheinen. Teleskopisch wäre er selbstverständlich nicht zu trennen. Sein Spektrum bestände aus der Übereinanderlagerung zweier, vielleicht total verschiedenartiger Spektren. Nach der Interferenzmethode müßte er als Doppelstern erscheinen. Alle Sterne, die von der Erde aus gesehen rings um A in der Entfernung $\gamma_0 - \beta$ liegen, würden von dem Stern A gleichsam eingefangen werden. Sollte zufällig TAB eine gerade Linie sein, so würde, von der Erde aus gesehen, der Stern A von einem Ring umgeben erscheinen.

Ob der hier angegebene Fall eines fiktiven Doppelsternes auch wirklich vorkommt, kann ich nicht beurteilen.

Petrograd, 1924 Jan. 28. *O. Chwolson.*

Antwort auf eine Bemerkung von *W. Anderson.*

Daß ein Elektronengas einer Substanz mit negativem Brechungsvermögen optisch äquivalent sein müßte, kann bei dem heutigen Stand unserer Kenntnisse nicht zweifelhaft sein, da dasselbe einer Substanz von verschwindend kleiner Eigenfrequenz äquivalent ist.

Aus der Bewegungsgleichung

$$\varepsilon X = \mu \, \mathrm{d}^2x/\mathrm{d}t^2$$

eines Elektrons von der elektrischen Masse ε und der ponderabeln Masse μ folgt nämlich für einen sinusartig pendelnden Prozeß von der Frequenz ν die Gleichung

$$\varepsilon X = -(2\pi\nu)^2 \mu x .$$

Berücksichtigt man, daß εx das »Moment« eines schwingenden Elektrons ist, so erhält man für die Polarisation $p = n\varepsilon x$ eines Elektronengases mit n Elektronen pro Volumeinheit

$$p = -\varepsilon^2 n/[\mu (2\pi\nu)^2] \cdot X .$$

Hieraus folgt, daß die scheinbare Dielektrizitätskonstante

$$D = 1 + 4\pi p/X = 1 - \varepsilon^2 n/(\pi\mu\nu^2)$$

ist. $\sqrt{D}$ ist in diesem Falle der Brechungsexponent, also jedenfalls kleiner als 1. Es erübrigt sich bei dieser Sachlage, auf das Quantitative einzugehen.

Es sei noch bemerkt, daß ein Vergleich des Elektronengases mit einem Metall unstatthaft ist, weil die bei der elementaren Theorie der Metalle zugrundegelegte »Reibungskraft« bei freien Elektronen fehlt; das Verhalten der letzteren ist allein durch die Einwirkung des elektrischen Feldes und durch die Trägheit bedingt.

Berlin, 1924 April 15. *A. Einstein.*

Zur Bemerkung von *W. Anderson* AN 5269.

In his note entitled »Zu Prof. *Einstein*s Bemerkung AN 5233«, *W. Anderson* makes use of the well-known formula for the index of refraction of a medium containing both free

of an electron gas is greater than unity, and that the conductivity is large. This assumption seems to be based on an erroneous conception of dielectric constant and conductivity. In fact, if *Hea-*

DISCUSSION

LENS-LIKE ACTION OF A STAR BY THE DEVIATION OF LIGHT IN THE GRAVITATIONAL FIELD

SOME time ago, R. W. Mandl paid me a visit and asked me to publish the results of a little calculation, which I had made at his request. This note complies with his wish.

The light coming from a star A traverses the gravitational field of another star B, whose radius is R_0. Let there be an observer at a distance D from B and at a distance x, small compared with D, from the extended central line $\overline{AB}$. According to the general theory of relativity, let α_0 be the deviation of the light ray passing the star B at a distance R_0 from its center.

For the sake of simplicity, let us assume that $\overline{AB}$ is large, compared with the distance D of the observer from the deviating star B. We also neglect the eclipse (geometrical obscuration) by the star B, which indeed is negligible in all practically important cases. To permit this, D has to be very large compared to the radius R_0 of the deviating star.

It follows from the law of deviation that an observer situated exactly on the extension of the central line $\overline{AB}$ will perceive, instead of a point-like star A, a luminius circle of the angular radius β around the center of B, where

$$\beta = \sqrt{\alpha_0 \frac{R_0}{D}}.$$

It should be noted that this angular diameter β does not decrease like $1/D$, but like $1/\sqrt{D}$, as the distance D increases.

Of course, there is no hope of observing this phenomenon directly. First, we shall scarcely ever approach closely enough to such a central line. Second, the angle β will defy the resolving power of our instruments. For, α_0 being of the order of magnitude of one second of arc, the angle R_0/D, under which the deviating star B is seen, is much smaller. Therefore, the light coming from the luminous circle can not be distinguished by an observer as geometrically different from that coming from the star B, but simply will manifest itself as increased apparent brightness of B.

The same will happen, if the observer is situated at a small distance x from the extended central line $\overline{AB}$. But then the observer will see A as two point-like light-sources, which are deviated from the true geometrical position of A by the angle β, approximately.

The apparent brightness of A will be increased by the lens-like action of the gravitational field of B in the ratio q. This q will be considerably larger than unity only if x is so small that the observed positions of A and B coincide, within the resolving power of our instruments. Simple geometric considerations lead to the expression

$$q = \frac{l}{x} \cdot \frac{1 + \frac{x^2}{2l^2}}{\sqrt{1 + \frac{x^2}{4l^2}}},$$

where

$$l = \sqrt{\alpha_0 D R_0}.$$

If we are interested mainly in the case $q \gg 1$, the formula

$$q = \frac{l}{x}$$

is a sufficient approximation, since $\frac{x^2}{l^2}$ may be neglected.

Even in the most favorable cases the length l is only a few light-seconds, and x must be small compared with this, if an appreciable increase of the apparent brightness of A is to be produced by the lens-like action of B.

Therefore, there is no great chance of observing this phenomenon, even if dazzling by the light of the much nearer star B is disregarded. This apparent amplification of q by the lens-like action of the star B is a most curious effect, not so much for its becoming infinite, with x vanishing, but since with increasing distance D of the observer not only does it not decrease, but even increases proportionally to $\sqrt{D}$.

ALBERT EINSTEIN

INSTITUTE FOR ADVANCED STUDY,
PRINCETON, N. J.

Alle Dreiecke sind gleichschenklig.

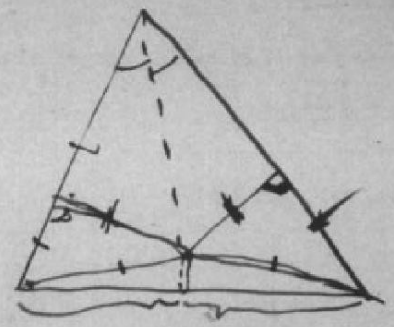

Herstellung
Berlin-Halensee,
Joachim Friedrichstr. 33.

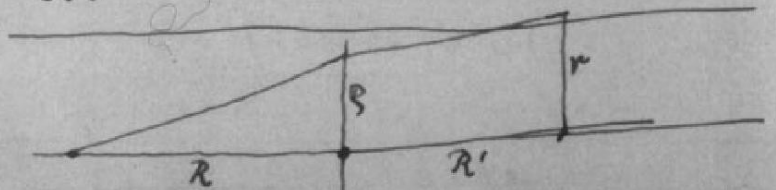

$$r = \varrho\frac{R+R'}{R} - \frac{R'\alpha}{\varrho}$$

$\varrho^2 r$ nach unten negativ. Dann gilt auch für stärkabgebogte Strahl.

$$r_0 = \varrho_0 - \frac{1}{\varrho_0} \quad \ldots (1)$$

$$\boxed{\varrho_0^2 = \varrho^2\frac{R+R'}{RR'\alpha}}$$

Einsetzg. $r = \cdot - \frac{R\alpha}{\varrho} = \cdot - \frac{R\alpha}{\varrho_0}\sqrt{\frac{R+R'}{RR'\alpha}}$

$$= \cdot - \frac{1}{\varrho_0}\sqrt{\frac{R}{R'}(R+R')\alpha}$$

$\neq$

$$\left.\begin{aligned} \boxed{r_0 = r\sqrt{\frac{R'}{R(R+R')\alpha}}} \\ \boxed{\varrho_0 = \varrho\sqrt{\frac{R+R'}{RR'\alpha}}} \end{aligned}\right\} (2)$$

1) gelt zwei Wurzeln für ϱ_0
Von hier an Index $_0$ weggelassen.

$$2 + r^2 = \varrho^2 + \frac{1}{\varrho^2}$$

$$f = \varphi + \frac{\pi^2}{\varphi}$$

$$df = \left(1 - \frac{\pi^2}{\varphi^2}\right)d\varphi = \left(1 - \frac{1}{\varrho^4}\right)d\varphi$$

$$\mathcal{H}df = \pm H\,d\varphi$$

$$\mathcal{H} = \pm\frac{H}{1 - \frac{1}{\varrho^4}}$$

$$\mathcal{H}_{tot} = H\left\{\frac{1}{1 - \frac{1}{\varrho_1^4}} + \frac{1}{\frac{1}{\varrho_2^4} - 1}\right\} \quad \ldots (3)$$

Klemmer gibt relative Helligkeit. (für ∞ = 1)

$$\frac{\varrho_1^4}{\varrho_2^2/M}$$

$$r = \frac{1}{x} - x$$

$$\{\ \} = \frac{1}{1 - x_1^4} + \frac{1}{x_2^4 - 1}$$

Nebulae as Gravitational Lenses

Einstein recently published[1] some calculations concerning a suggestion made by R. W. Mandl, namely, that a star B may act as a "gravitational lens" for light coming from another star A which lies closely enough on the line of sight behind B. As Einstein remarks the chance to observe this effect for stars is extremely small.

Last summer Dr. V. K. Zworykin (to whom the same idea had been suggested by Mr. Mandl) mentioned to me the possibility of an image formation through the action of gravitational fields. As a consequence I made some calculations which show that extragalactic *nebulae* offer a much better chance than *stars* for the observation of gravitational lens effects.

In the first place some of the massive and more concentrated nebulae may be expected to deflect light by as much as half a minute of arc. In the second place nebulae, in contradistinction to stars, possess apparent dimensions which are resolvable to very great distances.

Suppose that a distant globular nebula A whose diameter is 2ξ lies at a distance, a, which is great compared with the distance D of a nearby nebula B which lies exactly in front of A. The image of A under these circumstances is a luminous ring whose average apparent radius is $\beta=(\gamma_0 r_0/D)^{\frac{1}{2}}$, where γ_0 is the angle of deflection for light passing at a distance r_0 from B. The apparent width of the ring is $\Delta\beta=\xi/a$. The apparent total brightness of this luminous ring is q times greater than the brightness of the direct image of A. In our special case $q=2la/\xi D$, with $l=(\gamma_0 r_0 D)^{\frac{1}{2}}$. In actual cases the factor q may be as high as $q=100$, corresponding to an increase in brightness of five magnitudes. The surface brightness remains, of course, unchanged.

The discovery of images of nebulae which are formed through the gravitational fields of nearby nebulae would be of considerable interest for a number of reasons.

(1) It would furnish an additional test for the general theory of relativity.

(2) It would enable us to see nebulae at distances greater than those ordinarily reached by even the greatest telescopes. Any such *extension* of the known parts of the universe promises to throw very welcome new light on a number of cosmological problems.

(3) The problem of determining nebular masses at present has arrived at a stalemate. The mass of an average nebula until recently was thought to be of the order of $M_N=10^9 M_\odot$, where $M_\odot$ is the mass of the sun. This estimate is based on certain deductions drawn from data on the intrinsic brightness of nebulae as well as their spectrographic rotations. Some time ago, however, I showed[2] that a straightforward application of the virial theorem to the great cluster of nebulae in Coma leads to an average nebular mass four hundred times greater than the one mentioned, that is, $M_N'=4\times10^{11}M_\odot$. This result has recently been verified by an investigation of the Virgo cluster.[3] Observations on the deflection of light around nebulae may provide the most direct determination of nebular masses and clear up the above-mentioned discrepancy.

A detailed account of the problems sketched here will appear in *Helvetica Physica Acta*.

F. Zwicky

Norman Bridge Laboratory,
California Institute of Technology,
Pasadena, California,
January 14, 1937.

[1] A. Einstein, Science **84**, 506 (1936).
[2] F. Zwicky, Helv. Phys. Acta **6**, 124 (1933).
[3] Sinclair Smith, Astrophys. J. **83**, 23 (1936).

Emergence of Low Energy Protons from Nuclei

In some experiments recently described[1] the emission of protons in alpha-particle induced transmutations has been studied. In several cases the interesting fact was noticed that protons of relatively low energy were emitted in considerable numbers. Thus for each of the reactions

$$Al^{27}+He^4\rightarrow Si^{30}+H^1,$$
$$P^{31}+He^4\rightarrow S^{34}+H^1,$$
$$Cl^{35}+He^4\rightarrow A^{38}+H^1,$$
$$Ca^{40}+He^4\rightarrow Sc^{43}+H^1,$$

a group of protons of maximum range 20 cm or less is found and the yield is in general large (more than one-third of the total number of protons emitted). In each case protons of range 10 cm are observed with no apparent diminution of the probability of emission. The question arises as to how these low energy protons get out of the composite nucleus.

In recent experiments in this laboratory the excitation curve for the emission of neutrons from argon under alpha-particle bombardment has been plotted and the nuclear radius found to be 7.3×10^{-13} cm which is in accord with Bethe's revised radii for the radioactive elements[2] and may be taken as a basis for calculation of the nuclear radii of Si^{30}, S^{34}, A^{38}, Ca^{43} and Sc^{43}. Other evidence (e.g., scattering experiments) indicates, if anything, smaller radii than those found in this way. In Table I are given the radii so calculated, together with the heights of the corresponding proton barriers and the range of a proton just able to surmount them. It will be seen that in every case the experimentally observed ranges are smaller than necessary to scale the barrier. It therefore appears that we can draw one of two significant conclusions from the experimental data. Either *barriers to emerging protons are abnormally low* or *the composite nucleus containing the final product element and the proton has a finite lifetime sufficiently long to enable the proton to leak through the barrier*. The latter view, which is in accordance with Bohr's conception of transmutation,[3]

Table I.

Product Nucleus	Nuclear Radius ($\times10^{13}$cm)	Proton Barrier Height (Mev)	Range to Scale Barrier (cm)	Experimentally Found Range
Si^{30}	6.7	3.0	14.0	<10
S^{34}	6.9	3.3	16.5	<10
A^{38}	7.2	3.6	19.0	<10
Ca^{42}	7.4	3.9	22.0	14
Sc^{43}	7.5	4.0	23.0	<10

Constraints on DM objects from GL

(Wambsganss(1993))

Prefix	Deflection angle (")	Mass $M/M_\odot$	Lens	Time delay
kilo	10^3	10^{18}	supercluster	
macro	10^0	10^{12}	galaxy	months
milli	10^{-3}	10^6	MBH	min
micro	10^{-6}	10^0	star	10^{-4} sec
nano	10^{-9}	10^{-6}	planet	10^{-10} sec
pico	10^{-12}	10^{-12}	???	10^{-16} sec
femto	10^{-15}	10^{-18}	comet	10^{-22} sec

Just after the discovery of the first multiple imaged quasar QSO 0957+561 A,B by Walsh, Carswell & Weymann (1979) the idea of microlensing by low mass stars in heavy halo was suggested by Gott (1981).

First evidences of quasar microlensing was found by Irwin et al. (1989).

Now there are a number of known gravitational lens systems (Claeskens & Surdej 2002; Browne et al. 2003) and some of them indicate evidences for microlensing (Wambsganss 2001a).

Notations and expressions

$$\vec{\eta} = D_s\vec{\xi}/D_d - D_{ds}\vec{\Theta}(\vec{\xi}). \quad (5)$$

For Schwarzschild GL

$$\vec{\Theta}(\vec{\xi}) = 4GM\vec{\xi}/(c^2\xi^2). \quad (6)$$

If $\vec{\eta} = \vec{0}$ then

$$\xi_0 = \sqrt{\frac{4GM}{c^2} \times \frac{D_d D_{ds}}{D_s}}$$

is Einstein – Chwolson radius and

$$\theta_0 = \xi_0/D_d \quad (7)$$

is Einstein – Chwolson angle. If we introduce dimensionless variables $\vec{x} = \vec{\xi}/\xi_0, \vec{y} = D_s\vec{\eta}/(\xi_0 D_d)$ then

$$\vec{y} = \vec{x} - \vec{x}/x^2. \quad (8)$$

The Eq. (8) has two roots

$$\vec{x}^{\pm} = \vec{y}\left(\frac{1}{2} \pm \sqrt{\frac{1}{4} + \frac{1}{y^2}}\right) \quad (9)$$

and

$$l = |x^-| + |x^+| = 2y\sqrt{\frac{1}{4} + \frac{1}{y^2}}. \quad (10)$$

Astron. Astrophys. 260, 1–13 (1992)

ASTRONOMY AND ASTROPHYSICS

Research Note

The gravitational lens equation near cusps

P. Schneider and A. Weiss

Max-Planck-Institut für Astrophysik, Karl-Schwarzschild-Str. 1, W-8046 Garching bei München, Federal Republic of Germany

Received January 11, accepted February 29, 1992

Abstract. The behaviour of the gravitational lens mapping near cusps is studied, both analytically and numerically, paying particular attention to magnification probabilities. We demonstrate that the three images of a point source inside a cusp satisfy the relation that the sum of the magnifications of the two images with the same parity equals, up to a sign, the magnification of the third image (of opposite parity). This property will then be used to show that the asymptotic magnification cross-section for point sources, in the limit $\mu_s \to \infty$, derived previously for folds only, is also valid in the presence of cusps. The next order term of such an expansion, which is due to sources just outside of cusps, is derived. We apply these relations to a special gravitational lens model and show that these asymptotic relations are indeed very good approximations for the large-μ_s cross-sections. For the study of the magnification of extended sources near cusps, we generalize the ray-shooting method to allow for very small sources. The magnification cross-sections for extended sources are then compared to those for point sources. A magnification contour plot for extended sources near a cusp is obtained. Since the largest magnifications of sources occur near cusps, this paper may directly apply to studies of the amplification bias in source counts.

Key words: gravitational lensing, Catastrophe Theory

1. Introduction

The gravitational deflection of light, in the approximation of gravitational lens theory, can be described by a mapping $f : \mathbb{R}^2 \to \mathbb{R}^2$ from the lens plane (or a small part of the observer's sky) to the source plane (or the corresponding part of the sphere of constant source redshift). In the case of a single geometrically-thin deflector, this is a gradient mapping (for an introduction to gravitational lens theory, see Blandford & Narayan 1986, hereafter BN; Blandford & Kochanek 1987; Schneider, Ehlers & Falco 1992, hereafter SEF). The behaviour of such a gradient mapping near critical points, i.e., points where the Jacobian of the lens mapping vanishes, is investigated and classified by Catastrophe Theory (e.g., Poston & Steward 1978; Gilmore 1981; for applications in gravitational lensing, see BN; Kovner 1987a; SEF, Chap. 6). In a generic lens mapping, the critical points form closed, smooth, non-intersecting curves (so-called critical curves), and their image curves under the mapping f are the so-called caustics. They are also closed curves, but can intersect each other, self-intersect, and are not necessarily smooth, but can have cusps.

Caustics are an important ingredient in gravitational lens theory, for several reasons. First, the number of images of a source changes by ± 2 if, and only if, the source position changes across a caustic. Hence, knowing the structure of the caustics allows a qualitative understanding of the lens mapping, at least concerning image multiplicities. Also, if one considers families of lens mapping, Catastrophe Theory allows to predict the parameter values of the models at which the caustic structure changes, thus allowing a classification of parametrized lens models (for an example, see Erdl & Schneider 1992). Second, the magnification of a source, which is due to the area distortion of the lens mapping (i.e., the inverse of the Jacobian) becomes largest if the source is near a caustic. In particular, to determine the probability distribution for very large magnification of sources, one has to consider the lens mapping near caustics only.

A generic lens mapping has only two types of singularities, folds and cusps. At fold points, the caustic is smooth. A source on the "positive side" of a fold has two images close to, and on opposite sides of the corresponding critical curve. By approaching the caustic, the two critical images move closer together, thereby brightening. At the point where the source crosses the caustic, the two images attain (formally) infinite magnification (in practice, a finite source size leads to finite values of the magnification, but if we had a sufficiently compact source, wave optics effects would limit the magnification; see Chap. 7 of SEF and references therein), merge and disappear thereafter. The magnification of a point source scales like $1/\sqrt{y}$, where y is the distance of the source from the caustic. Considering folds only, the magnification probability of point sources in the limit of high magnifications, $\mu \to \infty$, behaves like μ^{-2}, and the constant of proportionality can be derived as a particular integral over the critical curves of the lens mapping (see BN, SEF, and Sect. 2.4 below).

The derivation of this probability distribution neglects the fact that cusps show a different behaviour. The standard argument implicitly used is that "cusps form a set of measure zero in the set of all critical points"; one therefore expects that cusps do neither change the shape, nor the amplitude of the $p(\mu) \propto \mu^{-2}$ law. Cusps are isolated points, connected by folds. A source close

Send offprint requests to: P. Schneider

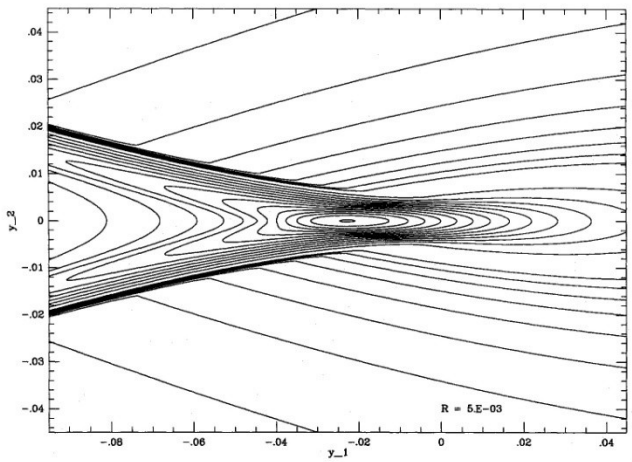

Fig. 5. Magnification contours around a generic cusp. The source radius chosen for this plot was $5\,10^{-3}$. The contour levels range from 3 to 10 in steps of one, and then to 80 (central contour) in steps of 5.

be the following: select a region in the source plane such that all points with magnification $> \mu_0$ lie inside the selected region (this region, in the case of the Chang-Refsdal lens, is preferentially chosen as a rectangle). Then, distribute N point sources inside this region (with area $\mathscr{A}$), calculate their magnifications from the lens equation, assign to each point a differential cross-section $d\sigma = \mathscr{A}/N$ and add up these differential cross-sections. If the N points are distributed randomly, we can easily estimate the number of points required for a given accuracy. If $\mathscr{A} \sim 4$, and $\sigma(10^3) \sim 4 \times 10^{-6}$ (typical values for the Chang-Refsdal lens), then $N_{1000} \sim 10^{-6} N$ points will have magnification $> 10^3$. If the cross-section is to be determined to within an accuracy of 10^{-3}, we would need $N = 10^{12}$ points — a hopeless task. The situation is slightly better if the points are not distributed randomly, but on a regular grid. Nevertheless, even then the computing time would be much too large for calculating accurate cross-sections for large μ_p.

To overcome these difficulties, we use a hierarchical method, based on the idea 'to use the computing time for interesting source positions'. For example, we want to distribute a higher density of points in regions where the magnification is large. Ideally, the number of source positions should be the same for each logarithmic bin of magnification, so that the statistical accuracy is smooth over the whole μ-interval considered. We now describe such a method applicable to point sources; a similar method has been used for extended sources, as described in the next subsection.

Consider the area $\mathscr{A}$ to be divided up into N squares. If the magnification at the center of a square is μ_p, we assign to this square a differential cross-section $d\sigma(\mu_p) = \mathscr{A}/N$. If this particular square is 'interesting' (we will specify this below), we can divide it into four subsquares and again calculate the magnification at the center of each subsquare (the corresponding differential cross-section then is $\mathscr{A}/(4N)$). If one or more of these subsquares appears again 'interesting', further divisions can be made; we can go down this hierarchy as far as desired.

Squares are 'interesting' if they have high magnification, if the gradient across the square is large, or if a caustic crosses the square (these conditions are not mutually exclusive, of course). We have defined numerical criteria according to the preceding prescription of 'interesting'; for example, if the magnification of a square at hierarchy level n is larger than μ_n, the square is further divided (it was found that $\mu_{n+1} = \mu_n\ 10^{0.15}$ is a good splitting criterium). Further, if the magnification factors at the corners of a square differed by more than 0.5, subdivision was applied. For the calculations shown in this paper, 14 hierarchy levels were used.

The solutions of the lens equation, and thus the point source magnification, can be calculated for the Chang-Refsdal lens, using the equations of Sect. 3. For each source position, one has to solve the fourth-order equation (3.3b), insert the real solutions into (3.3a), and calculate the magnification of each individual image. In connection with the hierarchical splitting of the source plane as described above, we have implemented an efficient and reliable method to solve Eq. (3.3a). This method will be described next; however, another method of solving the lens equation, to be described later, turned out to be superior in the situation considered here.

The Chang-Refsdal-equation in the form of Eq. (3.3b) can in principle be solved by any reasonable root-finder for polynomials or other well-behaved functions. Indeed, some of the root-solvers (e.g. from Press et al., 1986) worked well for most of the tested source positions, but with no exception all failed for those being close to cusps. The reason lies in the fact that at cusps a terrace point in the fourth-order polynomial $f(u)$ (given by (3.3b)) develops into a pair of extrema, or, in other words, a single root changes into three. All tested standard root-solvers gave the wrong number of roots of $f(u)$ on either side of the cusp! Numerically, a root cannot be found with an accuracy higher than $\approx 10^{-8}$ for coefficients of (3.3b) of the order of one by propagation of the machine inaccuracy into the powers of u.

Astron. Astrophys. 293, 1–4 (1995)

ASTRONOMY AND ASTROPHYSICS

On the magnification of gravitational lens images near cusps

Alexander F. Zakharov[1,2]

[1] Institute of Theoretical and Experimental Physics, B.Cheremushkinskaya, 25, 117259, Moscow, Russia
[2] Max-Planck-Institut für Astrophysik, Karl-Schwarzschild-Strasse 1, D-85740 Garching, Germany

Received 6 November 1993 / Accepted 30 April 1994

Abstract. On the base of the gravitational lens equation obtained by Schneider & Weiss the magnification of images near a cusp is investigated. Using the symmetrical polynomials on the roots of the polynomial of the third degree we slightly generalize the Schneider & Weiss statement on the magnification near different solutions of the gravitational lens equation. The analytical expressions for magnifications of different images near the cusp are presented.

Key words: gravitational lensing

1. Introduction

It is well known that the mapping of two-dimensional surfaces into a plane gives only two types of stable singularities: folds and cusps (pleats). There are also similar singularities of caustics in gravitational lens optics. Schneider & Weiss (1986; 1992) studied the gravitational lens mapping near the cusps. Mandzhos (1993) investigated the mutual coherence by solving analytically the gravitational lens equation near the cusp. In turn, we study the magnification near the cusp and obtain a useful analytical expression for it.

2. Basic equations

We recall the basic equations from Schneider & Weiss (1992) before considering their gravitational lens equation near the cusp. As is shown in Schneider, Ehlers & Falco (1992), hereafter SEF, the gravitational lens equation may be written in the following form: let the distance between an observer and a source be D_s, the distance between an observer and the gravitational lens be D_d , and D_{ds} be the distance between the gravitational lens and a source. If we suppose a small angle of deflection then we have the following simple expression for the lens equation (SEF)

$$\boldsymbol{\eta} = D_s\,\boldsymbol{\xi}/D_d + D_{ds}\,\boldsymbol{\beta}(\boldsymbol{\xi}),$$

Send offprint requests to: A.F. Zakharov

where the vectors $\boldsymbol{\eta}, \boldsymbol{\xi}$ define the coordinates in source plane and in the lens plane respectively (SEF),

$$\boldsymbol{\beta}(\boldsymbol{\xi}) = 4G/c^2 \int \rho\,(\boldsymbol{R})\,(\boldsymbol{\xi} - \boldsymbol{R})\,/\,|\,\boldsymbol{\xi} - \boldsymbol{R}|^2\,\mathrm{dXdY},$$

where $\boldsymbol{R}=\{X, Y\}$ is the point vector in the lens plane, $\rho(\boldsymbol{R})$ is the surface mass density of the gravitational lens. We introduce the following variables (SEF)

$$\boldsymbol{x} = \boldsymbol{\xi}/R_0, \quad \boldsymbol{y} = D_s\,\boldsymbol{\eta}/(R_0 D_d),$$

where $R_0 = \sqrt{2r_g D_d D_{ds}/D_s}$ is the Einstein - Chwolson radius (see Historical Remarks in SEF). We also introduce the following notation for the scaled (SEF) angle

$$\boldsymbol{\alpha} = \boldsymbol{\beta}\,D_{ds} D_d/(D_s R_0).$$

In the modelling of gravitational lenses, the surface mass density is normalized with the critical surface mass density (Wamsganss 1990)

$$\rho_{cr} = \frac{c^2 D_s}{4\pi G D_d D_{ds}}.$$

For typical lensing situations the critical surface mass density is of the order of $\rho_{cr} = 10^4 M_\odot \mathrm{pc}^{-2}$ (Wamsganss 1990). Therefore, if we define the scaled surface mass density by the following expression (SEF)

$$\sigma = \rho/\rho_{cr},$$

then we have the expression for the angle $\boldsymbol{\alpha}$

$$\boldsymbol{\alpha}(\boldsymbol{x}) = \int \sigma\,(\boldsymbol{x}')(\boldsymbol{x} - \boldsymbol{x}')/|\boldsymbol{x} - \boldsymbol{x}'|^2\,d^2x'.$$

As Schneider (1985) showed, we may introduce the scalar potential ψ, such, that

$$\boldsymbol{\alpha}(\boldsymbol{x}) = \nabla\psi\,(\boldsymbol{x}),$$

where

If we introduce (as in SEF)

$$\phi\,(\boldsymbol{x},\boldsymbol{y}) = (\boldsymbol{x}-\boldsymbol{y})^2/2 - \psi(\boldsymbol{x}),$$

we can write the lens equation in the form (Schneider 1985)

$$\nabla\phi\,(\boldsymbol{x},\boldsymbol{y}) = 0.$$

It is easy to see that mapping $x \mapsto y$ is a Lagrange mapping (Arnold 1979), since that is gradient mapping (Arnold 1983). Really, if we consider the function

$$S = \boldsymbol{x}^2\ /2 - \psi\,(\boldsymbol{x}),$$

then

$$\boldsymbol{y} = \nabla S.$$

Singularities of Lagrange's mappings are described in Arnold's paper (1972), and in Arnold's review (1983), and their bifurcations are described in Arnold's paper (1976).

Equation (1) defined the mapping of points on the lens plane into points on the source plane. Using the Jacobian matrix we define the local mapping (SEF):

$$\delta\,\boldsymbol{y} = A\,\delta\,\boldsymbol{x},$$

$$A = \begin{pmatrix} \partial y_1/\partial x_1 & \partial y_1/\partial x_2 \\ \partial y_2/\partial x_1 & \partial y_2/\partial x_2 \end{pmatrix} = \begin{pmatrix} 1-\psi_{11} & -\psi_{12} \\ -\psi_{21} & 1-\psi_{22} \end{pmatrix}, \qquad (2)$$

where

$$\psi_{ij} = \frac{\partial^2\psi}{\partial x_i \partial x_j}(i,j=1,2). \qquad (3)$$

Let us consider lenses which are systems of point masses. Outsides the points where the masses are located, we have the following equality (SEF)

$$\psi_{22} = -\psi_{11}, \qquad (4)$$

since the potential obeys the Laplace equation.

The magnification of an image at $\boldsymbol{x}$ is

$$\mu(\boldsymbol{x}) = 1/\det A\,(\boldsymbol{x}),$$

(where the mapping is not one-to-one). The set is formed by so-called critical curves (SEF).

Since $\det A(\gamma^{(c)}) = 0$ (at points on the critical curve), it is possible to find coordinates with $\phi_{11} \neq 0, \phi_{12} = \phi_{22} = 0$. As shown in Schneider & Weiss (1992), the lens equation near the cusp can be represented as

$$\begin{aligned} y_1 &= cx_1 + \frac{b}{2}x_2{}^2, \\ y_2 &= bx_1x_2 + ax_2{}^3, \end{aligned} \qquad (5)$$

where $a = \frac{1}{6}\phi_{2222}, b = \phi_{122}, c = \phi_{11}$ and $c \neq 0, b \neq 0, 2ac - b^2 \neq 0$. It was shown in SEF that additional terms do not affect the local properties of the mapping. It is possible to see that by the direct comparison of terms (for example the term with ϕ_{112} is smaller than the term with ϕ_{11}) or using Newton's polygon or Bruno's truncating rules (see for example Bruno 1989). Similar to Schneider & Weiss (1992), we introduce the notations

$$\hat{x}_1 = \frac{c}{b}x_1, \quad \hat{x}_2 = x_2, \quad \hat{y}_1 = y_1/b, \quad \hat{y}_2 = \frac{c}{b^2}y_2, \qquad (6)$$

then we have

$$\begin{aligned} \hat{y}_1 &= \hat{x}_1 + \frac{1}{2}\hat{x}_2^2, \\ \hat{y}_2 &= \hat{x}_1\hat{x}_2 + s\hat{x}_2^3, \end{aligned}$$

where $s = ac/b^2$. We also introduce $S = 1 - 2s$, $\tilde{y}_1 = 2\hat{y}_1/3S$, $\tilde{y}_2 = \hat{y}_2/S$; then we have (Schneider & Weiss 1992)

$$\hat{x}_1 = \frac{3S}{2}\tilde{y}_1 - \frac{1}{2}\hat{x}_2^2, \qquad (7)$$

$$\hat{x}_2^3 - 3\tilde{y}_1\hat{x}_2 + 2\tilde{y}_2 = 0. \qquad (8)$$

3. Statement on the magnifications of images near cusps

We recall that (Schneider & Weiss 1992)

$$\hat{\mu} = (\det\hat{A})^{-1}, \quad \hat{\mu} = b^2\mu, \qquad (9)$$

$$\det A = b^2 \det\hat{A} = b^2[\hat{x}_1 + (3s-1)\hat{x}_2^2]. \qquad (10)$$

Consider the magnifications for different images of one point inside the cusp. We show below that the following equality is valid for all sources inside the cusp

$$\hat{\mu}^{(1)} + \hat{\mu}^{(2)} + \hat{\mu}^{(3)} = 0. \qquad (11)$$

It is clear from Eq.(11) that we have the statement of Schneider & Weiss (1992) that

$$|\hat{\mu}^{(1)}| = |\hat{\mu}^{(2)} + \hat{\mu}^{(3)}|. \qquad (12)$$

It should be mentioned that Eq. (11) follows from Schneider and Weiss Eq.(2.3) (Eq. (12) of our paper) plus their comment on the parities after their Eq.(2.33b). We use the following expression for magnifications

$$\mu^{(i)} = \frac{1}{\hat{x}_1^{(i)} + (3s-1)(\hat{x}_2^{(i)})^2} \tag{13}$$

or using Eq.(7)

$$\mu^{(i)} = \frac{2}{S[\tilde{y}_1 - (\hat{x}_2^{(i)})^2]} \tag{14}$$

Therefore it is necessary to prove that

$$\frac{1}{\tilde{y}_1 - (\hat{x}_2^{(1)})^2} + \frac{1}{\tilde{y}_1 - (\hat{x}_2^{(2)})^2} + \frac{1}{\tilde{y}_1 - (\hat{x}_2^{(3)})^2} = 0 \tag{15}$$

or that

$$3\tilde{y}_1^2 - 2\tilde{y}_1[(\hat{x}_2^{(1)})^2 + (\hat{x}_2^{(2)})^2 + (\hat{x}_2^{(3)})^2] + \\ +[(\hat{x}_2^{(1)}\hat{x}_2^{(2)})^2 + (\hat{x}_2^{(1)}\hat{x}_2^{(3)})^2 + (\hat{x}_2^{(2)}\hat{x}_2^{(3)})^2] = 0. \tag{16}$$

Vieta's theorem applied to Eq.(8) yields

$$\hat{x}_2^{(1)} + \hat{x}_2^{(2)} + \hat{x}_2^{(3)} = 0,$$
$$\hat{x}_2^{(1)}\hat{x}_2^{(2)} + \hat{x}_2^{(1)}\hat{x}_2^{(3)} + \hat{x}_2^{(2)}\hat{x}_2^{(3)} = -3\tilde{y}_1.$$

If we express the symmetric power polynomials in terms of symmetric elementary polynomials we have

$$(\hat{x}_2^{(1)})^2 + (\hat{x}_2^{(2)})^2 + (\hat{x}_2^{(3)})^2 = 6\tilde{y}_1, \tag{17}$$
$$(\hat{x}_2^{(1)}\hat{x}_2^{(2)})^2 + (\hat{x}_2^{(1)}\hat{x}_2^{(3)})^2 + (\hat{x}_2^{(2)}\hat{x}_2^{(3)})^2 = 9\tilde{y}_1^2, \tag{18}$$

Thus we obtain (16). Similarly we have

$$q_1 = \hat{\mu}^{(1)}\hat{\mu}^{(2)}\hat{\mu}^{(3)} = \frac{2}{(3S)^3(\tilde{y}_1^3 - \tilde{y}_2^2)}, \tag{19}$$

$$p_1 = \hat{\mu}^{(1)}\hat{\mu}^{(2)} + \hat{\mu}^{(1)}\hat{\mu}^{(3)} + \hat{\mu}^{(2)}\hat{\mu}^{(3)} = \frac{-3\tilde{y}_1}{(3S)^2(\tilde{y}_1^3 - \tilde{y}_2^2)}. \tag{20}$$

Therefore we get an equation of third degree for the magnification of different images of a point inside the cusp

$$\tilde{\mu}^3 + \tilde{p}_1\tilde{\mu} + \tilde{q}_1 = 0, \tag{21}$$

where $\tilde{\mu} = \hat{\mu}/S, \tilde{p}_1 = p_1(3S)^2, \tilde{q}_1 = q_1(3S)^3$. If $\tilde{y}_1^3 > \tilde{y}_2^2$ then the discriminant for the pure cubic equation

$$D = \left(\frac{\tilde{p}_1}{3}\right)^3 + \left(\frac{\tilde{q}_1}{2}\right)^2 = \frac{-\tilde{y}_2^2}{(\tilde{y}_1^3 - \tilde{y}_2^2)^3}$$

is negative and we have three solutions of the Eq.(21) (see for example, Bronstein & Semendjajew 1980). Namely, we have

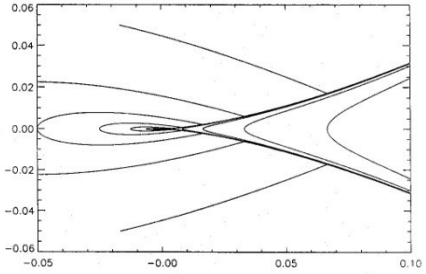

Fig. 1. Magnification contours around a cusp for the sum of absolute values of magnifications of all images. The contour levels are $10 * 2^i, -1 \le i \le 14$

for a point inside the cusp region

$$\tilde{\mu}^{(1)} = -\frac{2}{3}\sqrt{\frac{\tilde{y}_1}{\tilde{y}_1^3 - \tilde{y}_2^2}}\cos\left\{\frac{\cos^{-1}\left[\sqrt{\frac{\tilde{y}_1^3 - \tilde{y}_2^2}{\tilde{y}_1^3}}\right]}{3}\right\}, \tag{22}$$

$$\tilde{\mu}^{(2)} = -\frac{2}{3}\sqrt{\frac{\tilde{y}_1}{\tilde{y}_1^3 - \tilde{y}_2^2}}\cos\left\{\frac{\cos^{-1}\left[\sqrt{\frac{\tilde{y}_1^3 - \tilde{y}_2^2}{\tilde{y}_1^3}}\right]}{3} + \frac{2\pi}{3}\right\}, \tag{23}$$

$$\tilde{\mu}^{(3)} = -\frac{2}{3}\sqrt{\frac{\tilde{y}_1}{\tilde{y}_1^3 - \tilde{y}_2^2}}\cos\left\{\frac{\cos^{-1}\left[\sqrt{\frac{\tilde{y}_1^3 - \tilde{y}_2^2}{\tilde{y}_1^3}}\right]}{3} + \frac{4\pi}{3}\right\} \tag{24}$$

and we have only one solution for a point outside the cusp region

$$\tilde{\mu}^{(1)} = \frac{\sqrt[3]{\sqrt{\tilde{y}_2^2 - \tilde{y}_1^3} + \tilde{y}_2} + \sqrt[3]{\sqrt{\tilde{y}_2^2 - \tilde{y}_1^3} - \tilde{y}_2}}{\sqrt{\tilde{y}_2^2 - \tilde{y}_1^3}}. \tag{25}$$

It is possible to calculate the magnifications of the images from the direct solution of the gravitational lens equation near a cusp. Namely, we solve Eq.(8) and use Eqs.(7),(9),(10). After that we also obtain the expressions for magnifications.

4. Discussion

In Fig. 1 we present the contours for the sum of absolute values of magnifications of images near the cusp. Note that the algebraic sum of the values is equal to zero and that there are three real solutions of the gravitational lens equation in the cusp region. The contours are plotted by using expressions (22-25). It is possible to compare Fig. 1 with the similar figure from Schneider & Weiss (1992) that was obtained using the ray - shooting method (see, for example, Wamsganss 1990). Figure 1 shows clearly the cusp type singularity.

If we introduce $\vec{\theta} := \vec{\xi}/D_d, \vec{\beta} = \vec{\eta}/D_s$ then the magnification of GL mapping is

$$\mu := \frac{\Delta\omega}{\Delta\omega_0} := \left|\det \frac{\partial\vec{\beta}}{\partial\vec{\theta}}\right|^{-1} = \left|\det \frac{\partial\vec{y}}{\partial\vec{x}}\right|^{-1} \tag{11}$$

and

$$\mu_\pm = \frac{1}{4}\left(\frac{y}{\sqrt{4+y^2}} + \frac{\sqrt{4+y^2}}{y} \pm 2\right). \tag{12}$$

Therefore,

$$\mu_{\text{total}} = \mu_+ + \mu_- = \frac{y^2+2}{y(y^2+4)^{1/2}}, \tag{13}$$

thus $\mu_{\text{total}} \to 1/y$ (for $y \to 0$) and $\mu_{\text{total}} \to 1 + 1/y^4$ (for $y \to \infty$).

If $M \sim M_\odot$ and $D_d \sim 10$ kpc then

$$\theta_0 = 0.902\text{mas}\left(\frac{M}{M_\odot}\right)^{1/2}\left(\frac{10\text{ kpc}}{D_d}\right)\left(1 - \frac{D_d}{D_s}\right)^{1/2};$$

and angular velocity

$$\dot{\theta} = \frac{d\theta}{dt} = 4.22\left(\frac{v}{200\text{ km/s}}\right)\left(\frac{10\text{ kpc}}{D_d}\right)\frac{\text{mas}}{\text{yr}}. \tag{14}$$

Therefore a typical duration is

$$t_0 = \frac{\theta_0}{\dot{\theta}} = .214\left(\frac{M}{M_\odot}\right)^{1/2}\left(\frac{D_d}{10\ kpc}\right)^{1/2} \times \tag{15}$$

$$\times\left(1 - \frac{D_d}{D_s}\right)^{1/2}\left(\frac{200\text{ km/s}}{v}\right)\text{yr}. \tag{16}$$

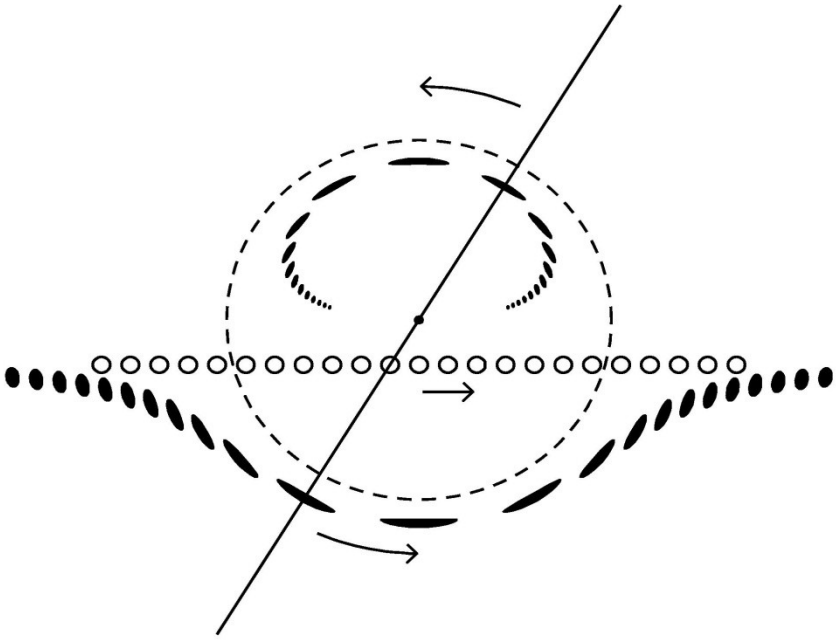

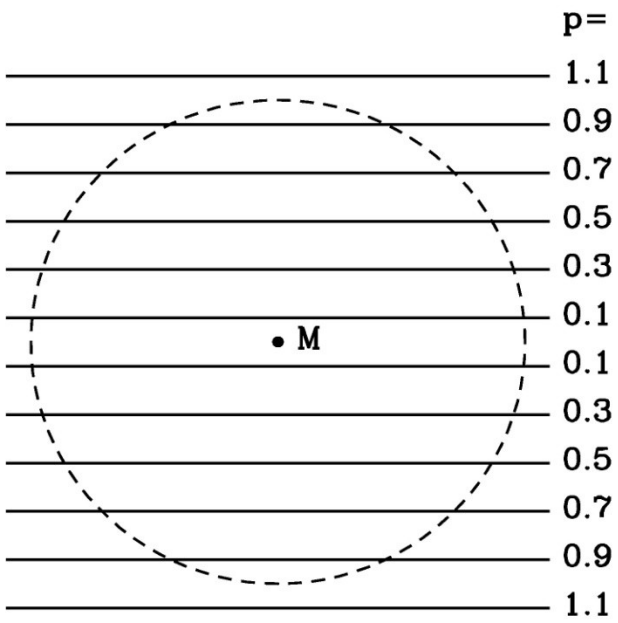
p=
1.1
0.9
0.7
0.5
0.3
0.1
M
0.1
0.3
0.5
0.7
0.9
1.1

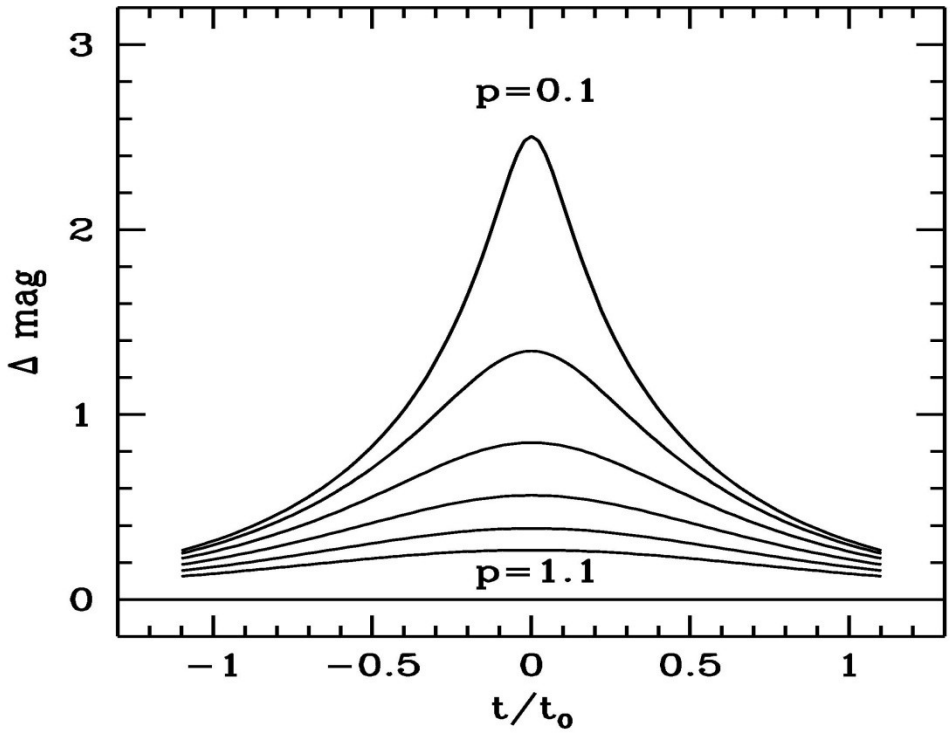
p=0.1
p=1.1
Δ mag
t/t_o
3
2
1
0
−1
−0.5
0
0.5
1

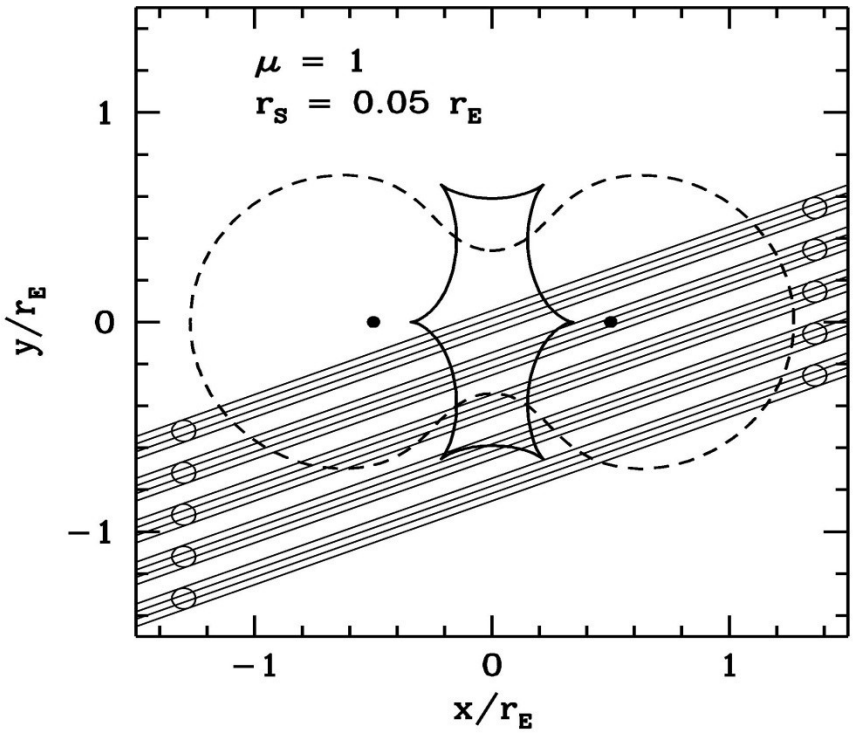
μ = 1
r_S = 0.05 r_E
1
0
−1
−1
0
1
y/r_E
x/r_E

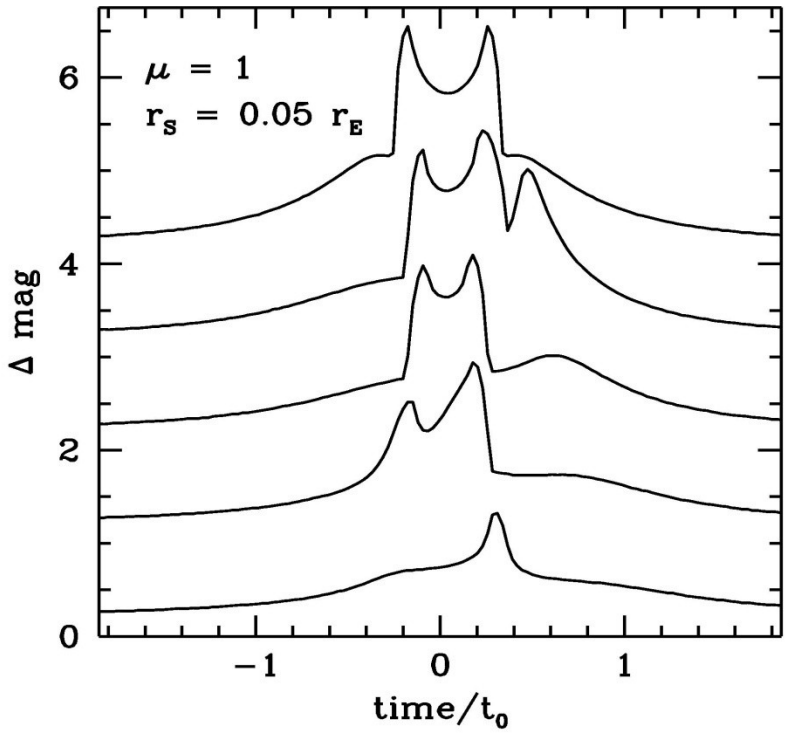
μ = 1
r_S = 0.05 r_E
Δ mag
6
4
2
0
−1
0
1
time/t_0

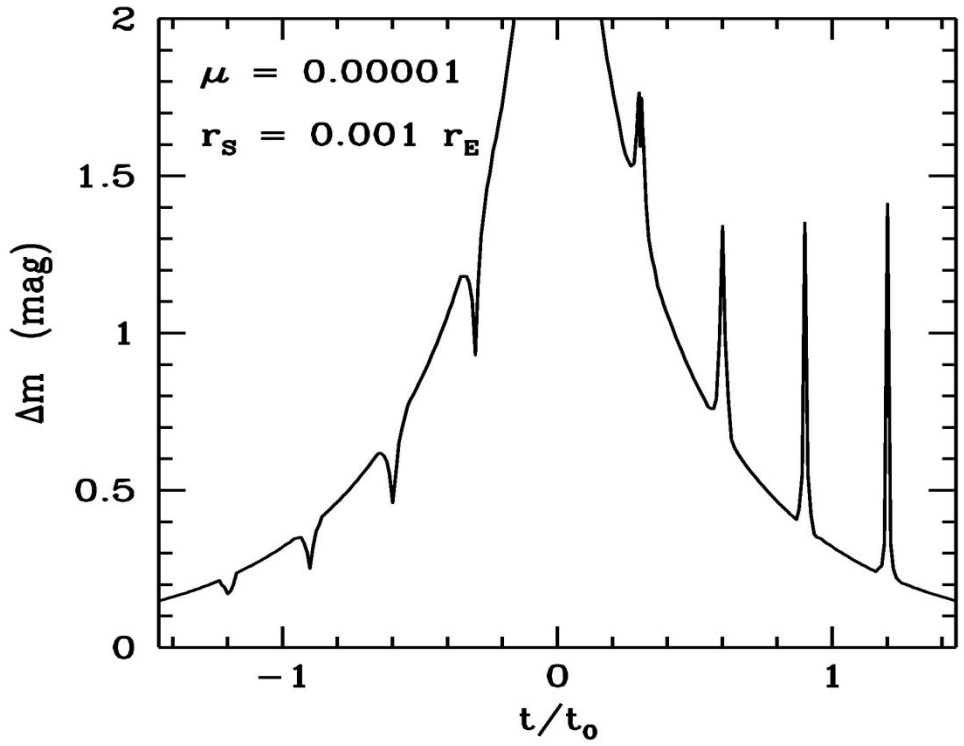
μ = 0.00001
r_S = 0.001 r_E
Δm (mag)
t/t_o
2
1.5
1
0.5
0
−1
0
1

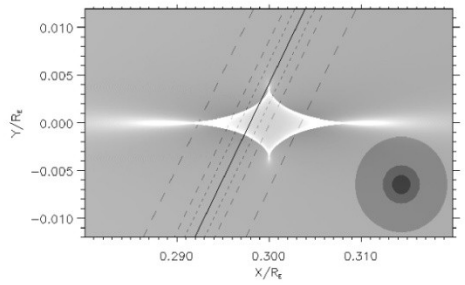
0.010
0.005
0.000
−0.005
−0.010
Y/R_E
0.290
0.300
0.310
X/R_E

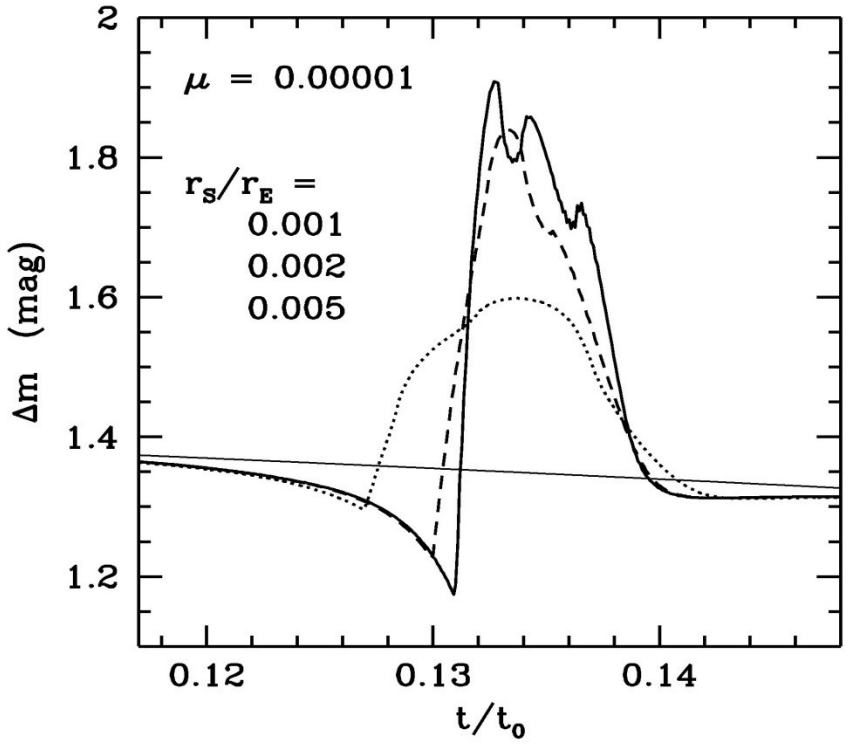
μ = 0.00001
r_S/r_E =
0.001
0.002
0.005
Δm (mag)
t/t_0
2
1.8
1.6
1.4
1.2
0.12
0.13
0.14

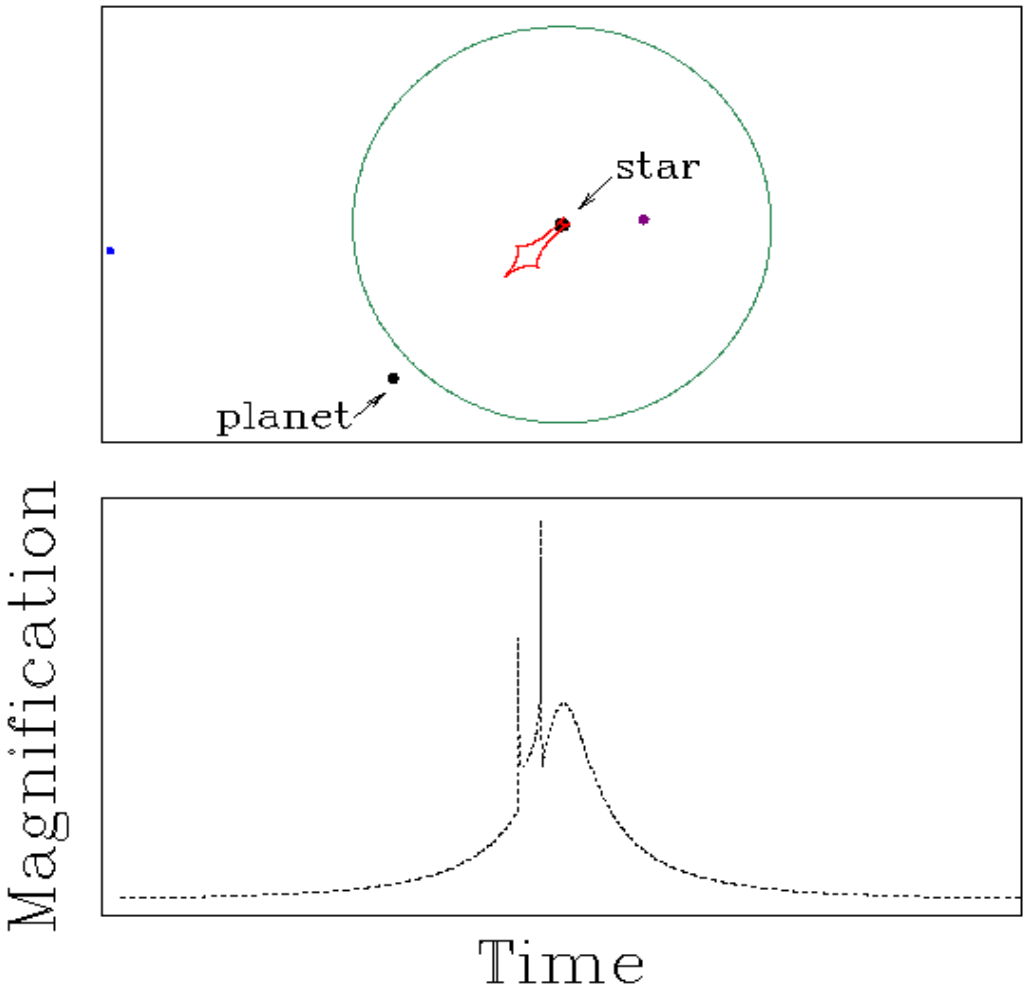
star
planet
Magnification
Time

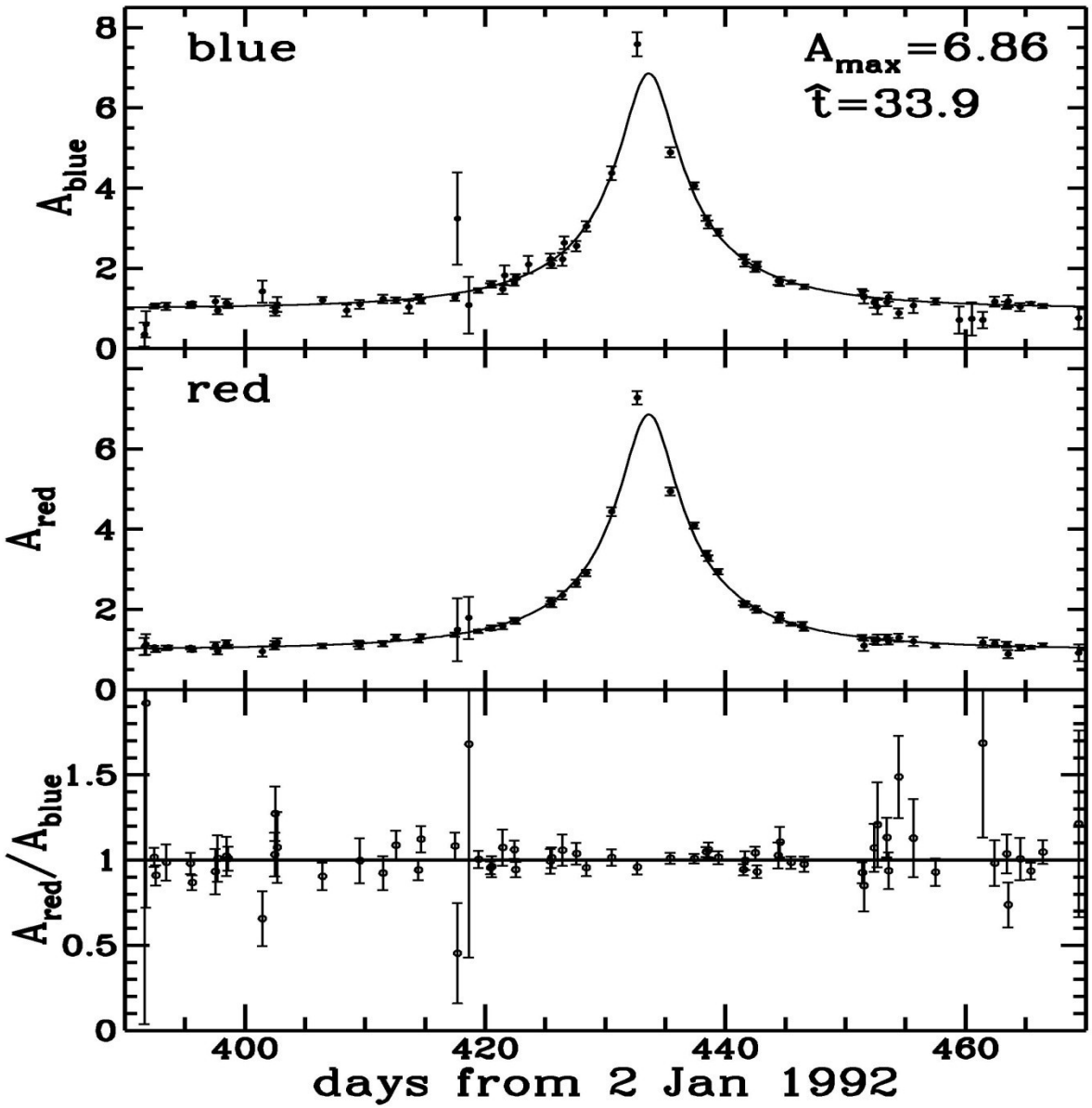
blue
A_{max}=6.86
$\hat{t}$=33.9
A_{blue}
red
A_{red}
A_{red}/A_{blue}
days from 2 Jan 1992

EROS collaboration (astro-ph/0011375)

Target: LMC & SMC

Time of observations: 3 years

Number of stars (10^6): 25

Number of candidates: 6 (1 (EROS-I); 4 (LMC), 1 (SMC) + 1 binary microlens in SMC). If the halo is formed by Machos with $M \sim M_\odot$, EROS could detect $\sim$ 30 events.

Durations of events (days): $24 - 44$

Probabilities:
$P(m \in [10^{-1}, 10] M_\odot \& f > 0.4) < 0.05$

Upper limit on the contribution of compact objects to the galactic halo

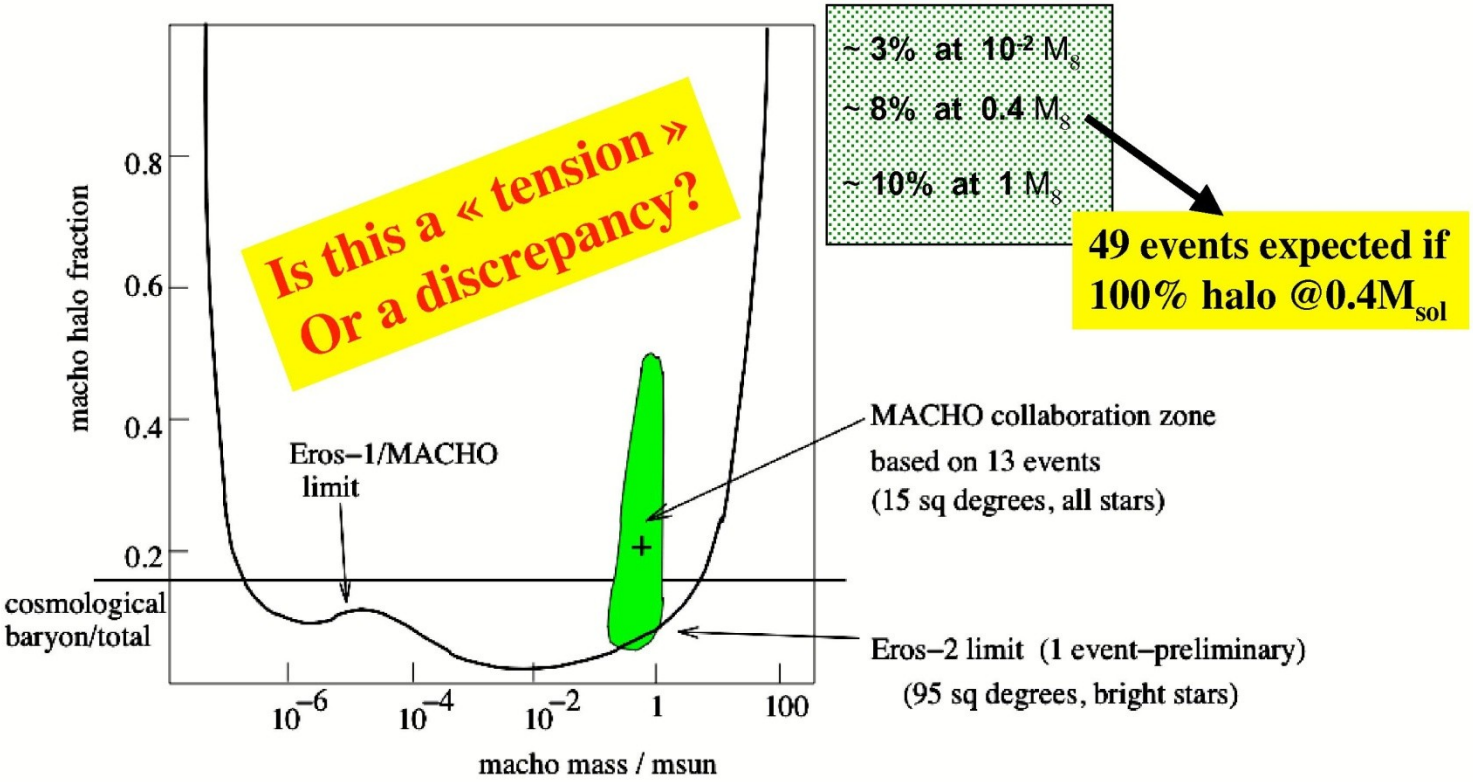

Planet discovery with ML with the lowest mass

(J.-P. Beaulieu et al. Nature, 2006)

Planet discovery with ML with the lowest mass in 2006 (now people find a planet with a mass about 2 Earth masses, see Mayor et al.)

(J.-P. Beaulieu et al. Nature, 2006)

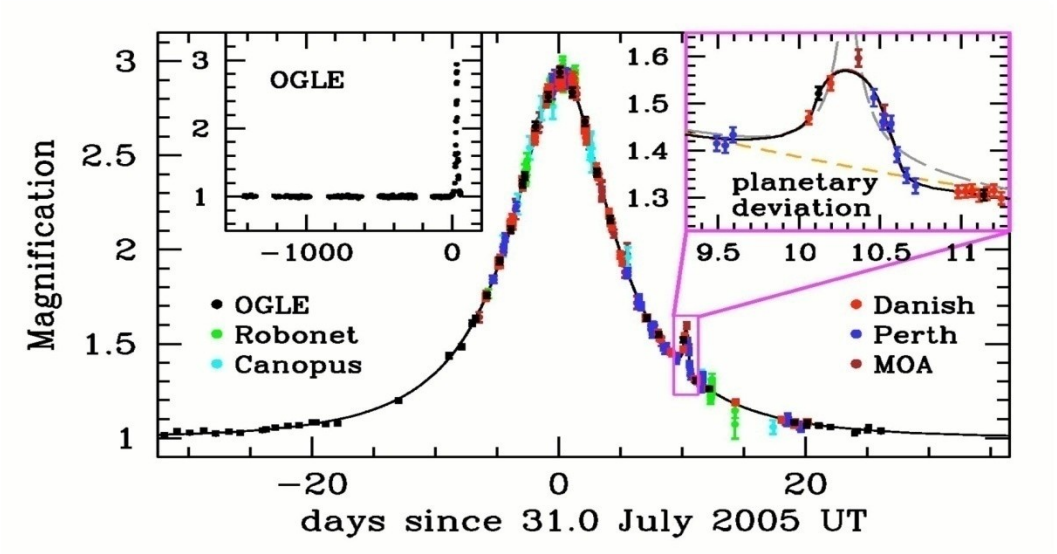

Figure 1 : The observed light curve of the OGLE-2005-BLG-390 microlensing event and best fit model plotted as a function of time. The data set consists of 650 data points from PLANET Danish (ESO La Silla, red points), PLANET Perth (blue), PLANET Canopus (Hobart, cyan), RoboNet Faulkes North (Hawaii, green), OGLE (Las Campanas, black), MOA (Mt John Observatory, brown). This photometric monitoring was done in the I band (with the exception of Faulkes R band data and MOA custom red passband) and real-time data reduction was performed with the different OGLE, PLANET and MOA data reduction pipelines. Danish and Perth data were finally reduced by the image subtraction technique[19] with the OGLE pipeline. The top left inset shows the OGLE light curve extending over the previous 4 years, whereas the top right one shows a zoom of the planetary deviation, covering a time interval of 1.5 days. The solid curve is the best binary lens model described in the text with a planet-to-star mass ratio of $q = 7.6 \pm 0.7 \times 10^{-5}$, and a projected separation $d = 1.610 \pm 0.008\ R_E$ (where R_E is the Einstein ring radius). The dashed grey curve is the best binary source model that is rejected by the data, while the dashed orange line is the best single lens model.

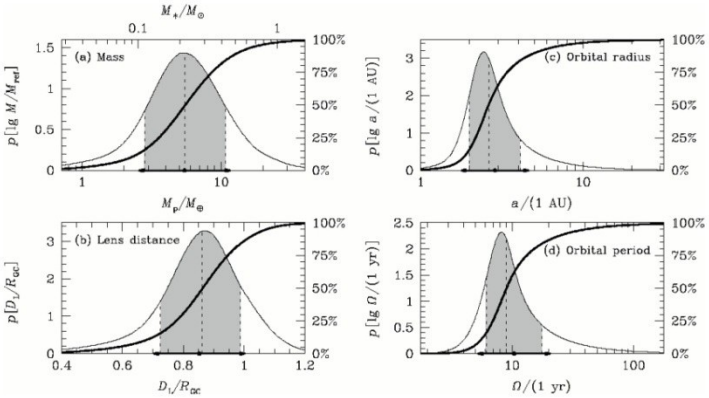

Figure 2 : Bayesian probability densities for the properties of the planet and its host star. The individual panels show the masses of the lens star and its planet (a), their distance from the observer (b), the three-dimensional separation or semi-major axis of an assumed circular planetary orbit (c) and the orbital period of the planet (d). The bold, curved line in each panel is the cumulative distribution, with the percentiles listed on the right. The dashed vertical lines indicate the medians, and the shading indicates the central 68.3% confidence intervals, while dots and arrows on the abscissa mark the expectation value and standard deviation. All estimates follow from a Bayesian analysis assuming a standard model for the disk and bulge population of the Milky Way and the stellar mass function of ref. [23], and a prior for the source distance D_S=1.05 ±0.25 R_{GC} (where R_{GC}= 7.62 ± 0.32 kpc for the Galactic Centre distance). The medians of these distributions yield a $5.5^{+5.5}_{-2.7}$ Earth mass planetary companion at a separation of $2.6^{+1.5}_{-0.6}$ AU from a $0.22^{+0.21}_{-0.11} M_{\odot}$ Galactic Bulge M-dwarf at a distance of 6.6 ± 1.0 kpc from the Sun. The median planetary period is 9^{+9}_{-3} years. The logarithmic means of these probability distributions (which obey Kepler's third law) are a separation of 2.9 AU, a period of 10.4 years, and masses of $0.22M_{\odot}$ and $5.5M_{\oplus}$ for the star and planet, respectively. In each plot, the independent variable for the probability density is listed within square brackets. The distribution of planet-star mass ratio was taken to be independent of the stellar mass, and a uniform prior was assumed for the planet-star separation distribution.

D.P. Bennett et al. A Low-Mass Planet with a Possible Sub-Stellar-Mass Host in Microlensing Event MOA-2007-BLG-192
Arxive:0806.0025[astro-ph] .

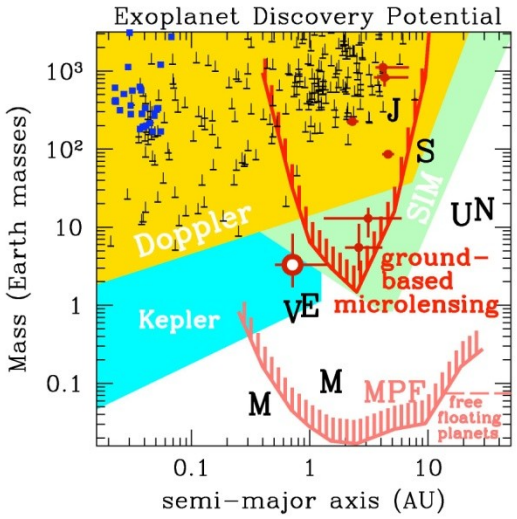

Fig. 16.— The known extrasolar planets are plotted as a function of mass vs. semi-major axis, along with the predicted sensitivity curves for a number of methods. The microlensing planets are indicated by dark red spots with error bars, and the large red spot with a white dot in the center is MOA-2007-BLG-192Lb. The blue dots indicate the planets first detected via transits, and the black bars with upward pointing error bars are the radial velocity planet detections. (The upward error bars indicate the 1-σ $\sin i$ uncertainty.) The gold, cyan, and light green shaded regions indicated the expected sensitivity of the radial velocity programs and the Kepler and SIM space missions. The dark and light red curves indicate the predicted lower sensitivity limits for a ground based and space-based (Bennett & Rhie 2002) microlensing planet search program, respectively. The Solar System's planets are indicated with black letters.

The POINT-AGAPE collaboration

(Pixels Observation at INT) (Andromeda Galaxy Amplified Pixel Experiment)

ARI – Liverpool, IoA – Cambridge, ITP – Zurich, OMP – Toulouse, Oxford University
PCC-Collège de France – Paris, QWM – London, Université Bretagne-sud – Vannes

Photometric survey of M31:

- Isaac Newton Telescope (INT) ∅=2,5m (La Palma, Canaries)
- Wide Field Camera (WFC)
- 180 observation nights (1 h/night between aug. 1999 and jan. 2002)
- 3 filters : Sloan i', r' et g'
- field : 0,55 deg²

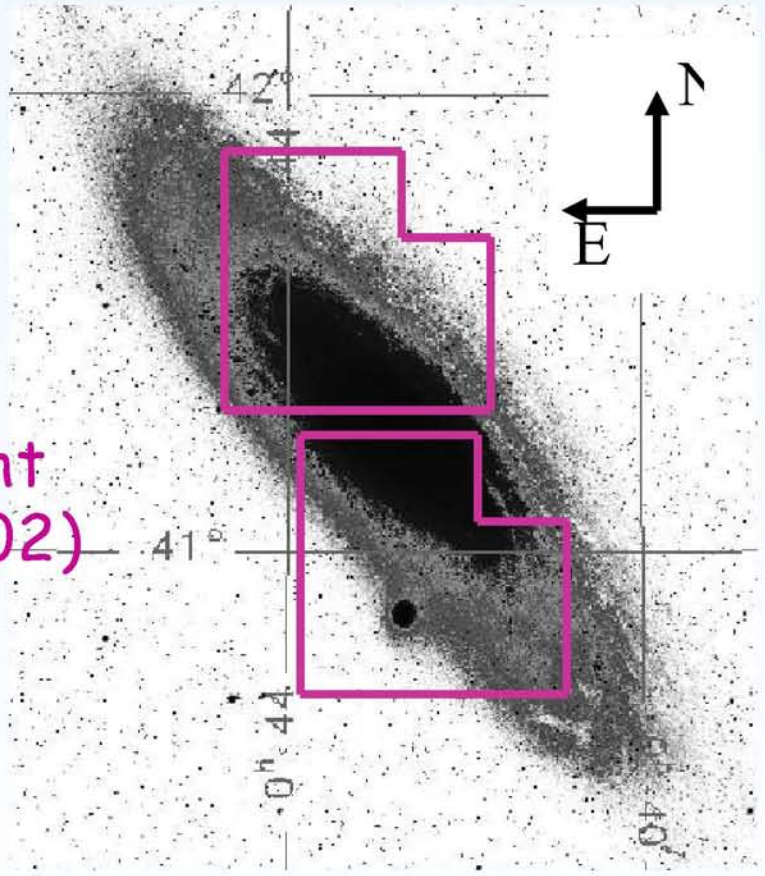

7 bright-short microlensing events

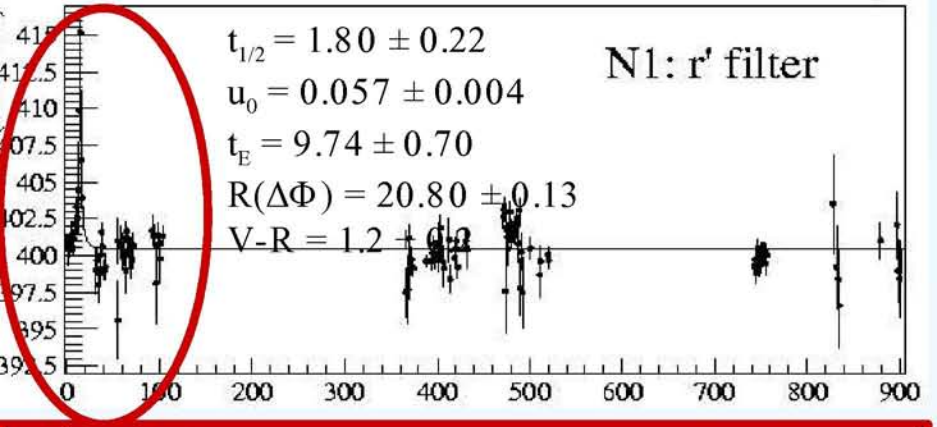

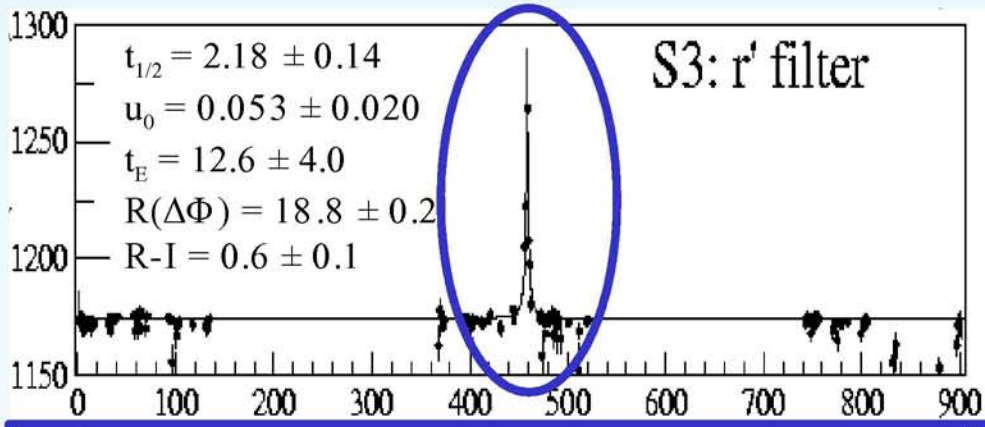

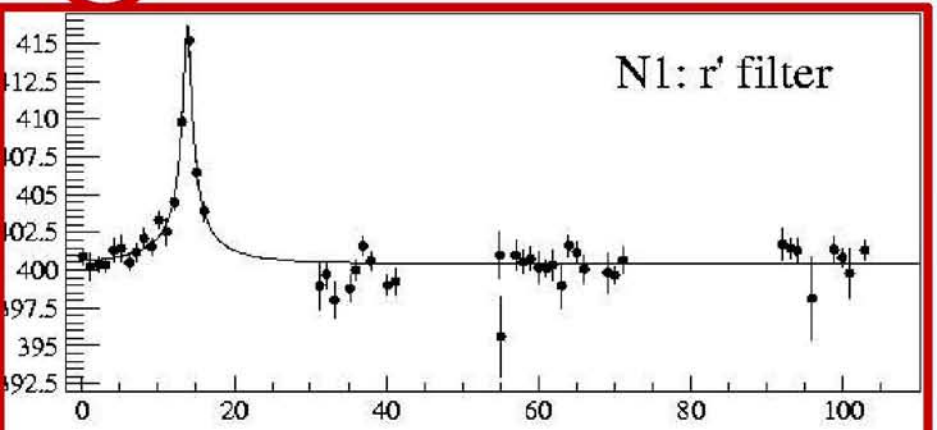

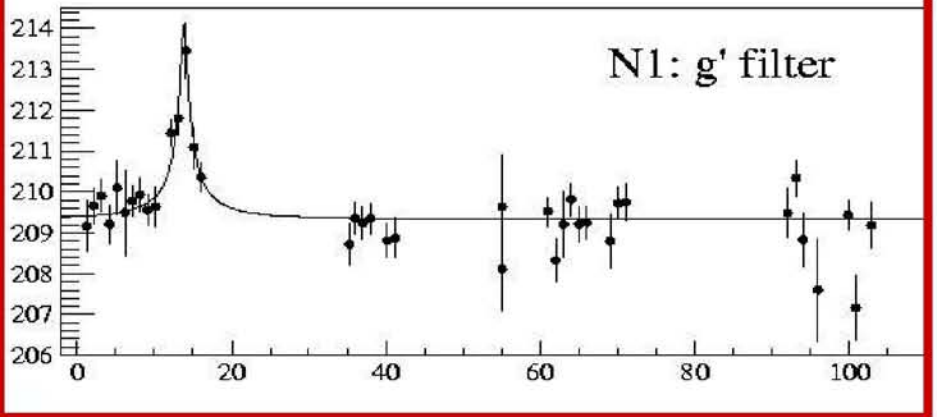

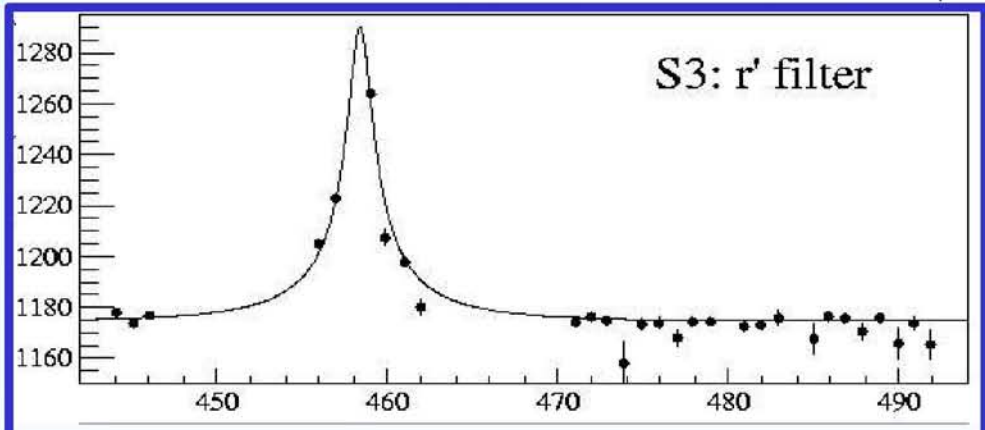

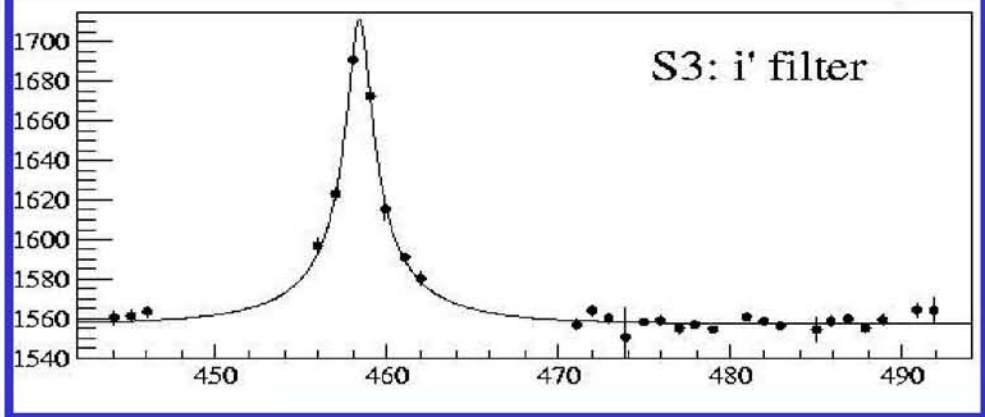

A&A 432, 501–513 (2005)
DOI: 10.1051/0004-6361:20041355

Astronomy & Astrophysics

Influence of magnification threshold on pixel lensing optical depth, event rate and time scale distributions towards M 31

F. De Paolis[1], G. Ingrosso[1], A. A. Nucita[1], and A. F. Zakharov[2,3]

[1] Dipartimento di Fisica, Università di Lecce and INFN, Sezione di Lecce, CP 193, 73100 Lecce, Italy
e-mail: ingrosso@le.infn.it
[2] Institute of Theoretical and Experimental Physics, 25, B. Cheremushkinskaya St., Moscow 117259, Russia
[3] Astro Space Centre of Lebedev Physics Institute, Moscow

Received 26 May 2004 / Accepted 2 November 2004

Abstract. Pixel lensing is the gravitational microlensing of light from unresolved stars contributing to the luminosity flux collected by a single pixel. A star must be sufficiently magnified, that is, the lens impact parameter must be less than a threshold value u_T if the excess photon flux in a pixel is to be detected over the background. Assuming the parameters of the Isaac Newton Telescope and typical observing conditions, we present maps in the sky plane towards M 31 of threshold impact parameter, optical depth, event number and event time scale, analyzing in particular how these quantities depend on u_T in pixel lensing searches. We use an analytical approach consisting of averaging on u_T and the star column density the optical depth, microlensing rate and event duration time scale. An overall decrease in the expected optical depth and event number with respect to the classical microlensing results is found, particularly towards the high luminosity M 31 inner regions. As expected, pixel lensing events towards the inner region of M 31 are mostly due to self-lensing, while in the outer region dark events dominate even for a 20% MACHO halo fraction. We also find a far-disk/near-disk asymmetry in the expected event number, smaller than that found by Kerins (2004). Both for self and dark lensing events, the pixel lensing time scale we obtain is $\simeq$1−7 days, dark events lasting roughly twice as long as self-lensing events. The shortest events are found to occur towards the M 31 South Semisphere. We also note that the pixel lensing results depend on $\langle u_T \rangle$ and $\langle u_T^2 \rangle$ values and ultimately on the observing conditions and telescope capabilities.

Key words. gravitational lensing – Galaxy: halo – cosmology: dark matter – galaxies: individual: M 31 – methods: observational

1. Introduction

Pixel lensing surveys towards M 31 (Crotts 1992; Baillon et al. 1993) can give valuable information to probe the nature of MACHOs (Massive Astrophysical Compact Halo Objects) discovered in microlensing experiments towards the LMC and SMC (Large and Small Magellanic Clouds) (Alcock et al. 1993; Aubourg et al. 1993) and also address the question of the fraction of halo dark matter in the form of MACHOs in spiral galaxies (Alcock et al. 2000).

This may be possible due to both the increase in the number of expected events and because the M 31 disk is highly inclined with respect to the line of sight and so microlensing by MACHOs distributed in a roughly spherical M 31 halo give rise to an unambiguous signature: an excess of events on the far side of the M 31 disk relative to the near side (Crotts 1992).

Moreover, M 31 surveys probe the MACHO distribution in a different direction to the LMC and SMC and observations are made from the North Earth hemisphere, probing the entire halo extension.

The Pixel lensing technique studies the gravitational microlensing of unresolved stars (Ansari et al. 1997). In a dense field of stars, many of them contribute to each pixel. However, if one unresolved star is sufficiently magnified, the increase of the total flux will be large enough to be detected. Therefore, instead of monitoring individual stars as in classical microlensing, one follows the luminosity intensity of each pixel in the image. When a significative (above the background and the pixel noise) photon number excess repeatedly occurs, it is attributed to an ongoing microlensing event if the pixel luminosity curve follows (as a function of time) a Paczynski like curve (Paczynski 1996).

Clearly, variable stars could mimic a microlensing curve. These events can be recognized by performing observations in several spectral bands and monitoring the signal from the same pixel for several observing seasons to identify the source.

Two collaborations, MEGA (preceded by the VATT/Columbia survey) and AGAPE have produced a number of microlensing event candidates, which show a rise in pixel luminosity in M 31 (Crotts & Tomaney 1996; Ansari et al. 1999; Auriere et al. 2001; Calchi Novati et al. 2002).

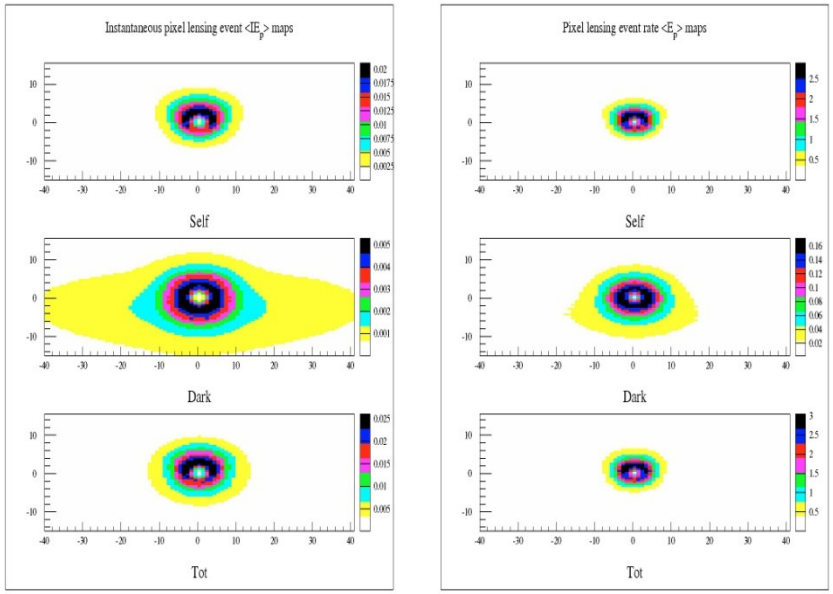

Fig. 5. In panel **a)**, the instantaneous pixel lensing event number density $\langle IE_{\rm p}(x,y)\rangle$ maps (events per arcmin^2) towards M 31 are given for self, dark and total lensing. In panel **b)** maps of pixel lensing event rate $\langle E_{\rm p}(x,y)\rangle$ (events per year and per arcmin^2) are given, in the same cases.

expected total number of events detectable by monitoring for 1 year the 100×70 arcmin^2 region oriented along the major axis of M 31 (events within 8 arcmin from the center are excluded). The first four lines refer to the models considered in Table 1 and to the parameters in the third row of Table 2. As one can see, the obtained results for the Reference model are intermediate with respect to those for the other more extreme models.

In the last row of Table 3, for the Reference model we show how the expected event number changes considering a different value of $\langle u_{\rm T}\rangle_\phi \simeq 1.44 \times 10^{-2}$ (see 5th row in Table 2). As expected, one can verify that roughly the event number scales as $\langle u_{\rm T}\rangle_\phi$.

Similar results have been obtained in previous simulations (see, e.g. Kerins 2004, and references therein). We also note that our numerical results scale with the fraction of halo dark matter in form of MACHOs and with the MACHO mass by a factor $(f_{\rm MACHO}/0.2)\ \sqrt{0.5\ M_\odot/m_{\rm l}}$.

In Table 4 we give the total event number $\langle E_{\rm p}\rangle$ for different lens populations (bulge, disk and halo) located in M 31. As one can see, the ratio dark/total events depends on the considered model, varying from 0.07 (for the massive disk model) to 0.40 for the massive halo model.

To study the far-disk/near-disk asymmetry, in the last three columns of Table 4 we give results for the South/North M 31 Semispheres and in brackets their ratio. For the Reference model, we find that self-lensing events are roughly symmetric (the same is true for lenses located in the MW disk and halo, not given in the table), while events due to lenses in M 31 halo are asymmetrically distributed with a ratio of about 2. The asymmetry is particularly evident (in the last column of the table) for sources located in the disk.

In Table 5 the instantaneous total number of events $\langle IE_{\rm p}\rangle$ within the considered M 31 region is given. The first four rows refer to the parameter values $\langle m_{\rm b}\rangle \simeq 0.31\ M_\odot$, $\langle m_{\rm d}\rangle \simeq 0.53\ M_\odot$, $f_{\rm MACHO} = 0.2$ and $\langle u_{\rm T}^2\rangle_\phi \simeq 9.56 \times 10^{-3}$ (used throughout the paper). For comparison with the results obtained by Kerins (2004), in the last four rows of Table 5 we present our results for $\langle m_{\rm b}\rangle \simeq 0.5\ M_\odot$, $\langle m_{\rm d}\rangle \simeq 0.5\ M_\odot$, $f_{\rm MACHO} = 1$ and $\langle u_{\rm T}^2\rangle_\phi \simeq 1.17 \times 10^{-3}$. The asymmetry ratio we obtain is always rather smaller than that quoted by Kerins (2004).

As it has been mentioned by several authors, in order to discriminate between self and dark lensing events, it is important to analyze the event duration. Indeed self-lensing events are expected to have, on average, shorter duration with respect to events due to halo MACHOs.

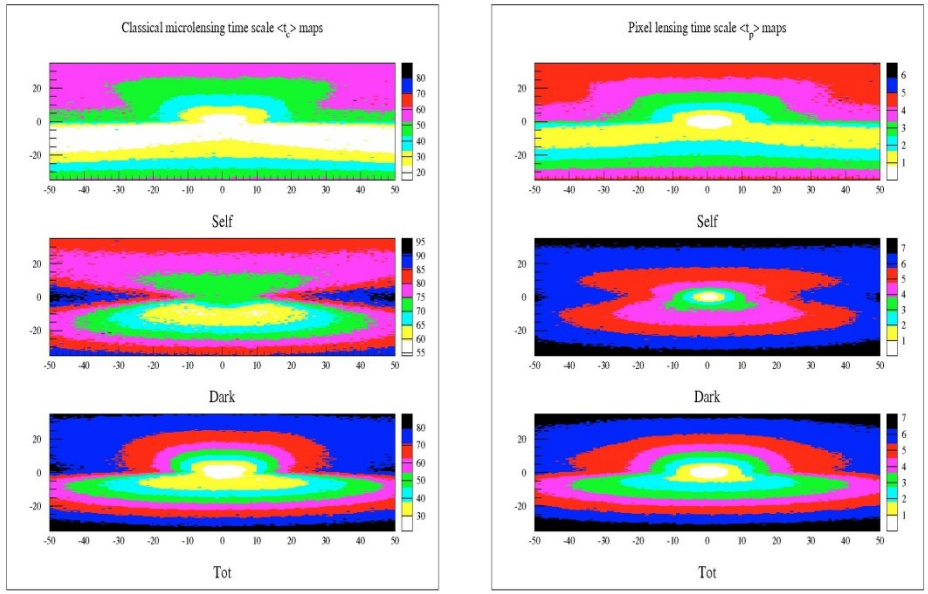

Fig. 6. In panel **a)**, mean classical event duration time $\langle t_c(x,y)\rangle$ (in days) maps towards M 31 are given for self, dark and total lensing. In panel **b)** for pixel lensing, maps of $\langle t_p(x,y)\rangle$ are given, in the same cases.

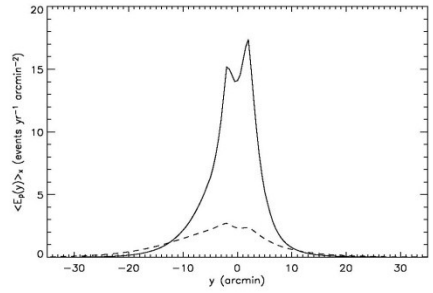

Fig. 7. The projected (along the x axis) mean event number $\langle E_p(y)\rangle_x$ is given as a function of the coordinate y for the Reference model. The dashed line refers to dark lensing events by MACHOs in M 31 and MW halos while the solid line is for self-lensing events by stars in M 31 bulge and disk.

6.4. Pixel lensing event time scale

Maps of mean event duration time scale in classical and pixel lensing are shown in Figs. 6a and 6b.

Here we use the probability, for each location of sources and lenses given in Eq. (26), of obtaining event duration maps for self and dark microlensing events.

As expected, short duration events are mainly distributed towards the inner regions of the galaxy and this occurs for both $\langle t_c(x,y)\rangle$ and $\langle t_p(x,y)\rangle$. The main effect of $\langle u_T(x,y)\rangle_\phi$ is to decrease the event time scale, in particular towards the inner regions of M 31, giving a larger number of short duration events with respect to expectations based on $\langle t_c(x,y)\rangle$ calculations.

Both for self and dark events the pixel lensing time scale we obtain is $\simeq$1−7 days, in agreement with results in Kerins (2004), but much shorter with respect to the duration of the events observed by the MEGA Collaboration (de Jong et al. 2004). This is most likely due to the fact that current experiments may not detect events shorter than a few days.

However, the pixel lensing time scale values depend on $\langle u_T(x,y)\rangle_\phi$ and ultimately on the observational conditions and the adopted analysis procedure. Indeed from Table 2 one can see that the $\langle u_T(x,y)\rangle_\phi$ value may be easily doubled, changing the adopted parameters and therefore giving longer events.

In Fig. 8 the pixel lensing event duration $\langle t_p(y)\rangle$ averaged along the x direction is given as a function of the y coordinate. The dashed line refers to dark lensing events by MACHOs

Pixel-lensing and extra-solar searches
G. Ingrosso, S. Calchi-Novati, F. De Paolis, P. Jetzer, A. Nucita, AFZ (MNRAS, in press, arXiv:0906.1050)

Planets with masses 0.1 Earth masses may be detected in M31


NASA

Hint of planet outside our galaxy

By Jason Palmer
Science and technology reporter, BBC News

Astronomers believe they have seen hints of the first planet to be spotted outside of our galaxy.

Situated in the Andromeda galaxy, the planet appears to be about six times the mass of Jupiter.

The method hinges on gravitational lensing, whereby a nearer object can bend the light of a distant star when the two align with an observer.

The results will be published in Monthly Notices of the Royal Astronomical Society (MNRAS).

The team, made up of researchers from the National Institute of Nuclear Physics (INFN) in Italy and collaborators in Switzerland, Spain, and Russia, exploited a type of gravitational lensing called microlensing.

The effect of large, massive objects between an observer and a distant planet or star can cause distortion or multiple images as the

AP/NASA

First Planet in Another Galaxy Possibly Found

Friday, June 12, 2009

FOX NEWS

The Andromeda galaxy in a NASA composite image.

Astronomers may have found the first planet in another galaxy, according to New Scientist magazine.

Planet : PA-99-N2 b

THE PLANET

Basic data :

Name	PA-99-N2 b
Discovered in	2009
M.sin *i*	6.34 M_J
Update	16/06/09

http://exoplanet.eu/planet.php?p1=PA-99-N2&p2=b&showPubli=yes&sortByDate

Remarks :

Reanalysis of data by An et al 2004

2 related publications : (sort by author) (sort by date)

AN J., EVANS N., KERINS E., BAILLON P., CALCHI NOVATI S., CARR J., CREZE M., GIRAUD-HERAUD Y., GOULD A., HEWETT P., JETZER Ph., KAPLAN J., PAULIN-HENRIKSSON S., SMARTT S., TSAPRAS Y. & VALLS-GABAUD D. (The POINT-AGAPE Collaboration) , 2004

The anomaly in the candidate microlensing event PA-99-N2

ApJ. , **601** , 845

paper

INGROSSO G., CALCHI NOVATI S., DE PAOLIS F., JETZER Ph., NUCITA A. & ZAKHAROV A. , 2009

Pixel-lensing as a way to detect extrasolar planets in M31

MNRAS , **-** , -

accepted

preprint

THE STAR
in M31

Name	PA-99N2
Distance	670000 *pc*
Mass	0.5 M_{sun}

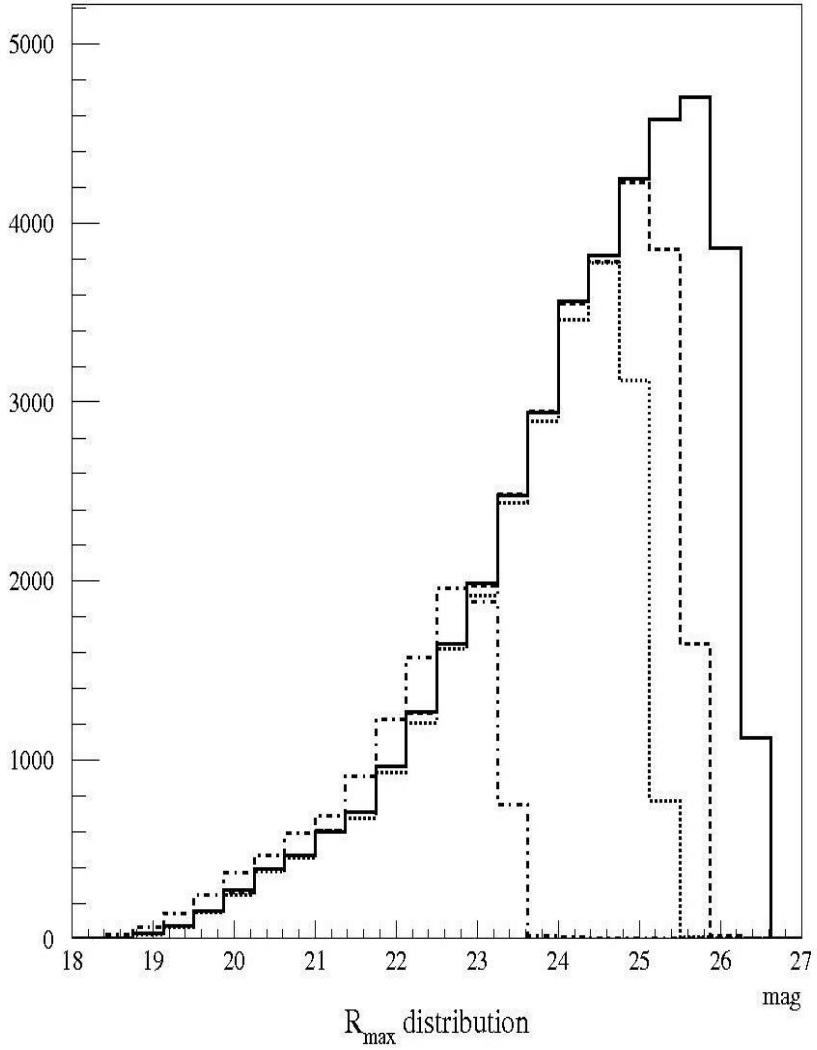

Figure 1. Normalised distributions of R_{max} for detectable pixel-lensing events with telescopes having different sizes $D =$ 1.5, 2.5, 4, 8 m.

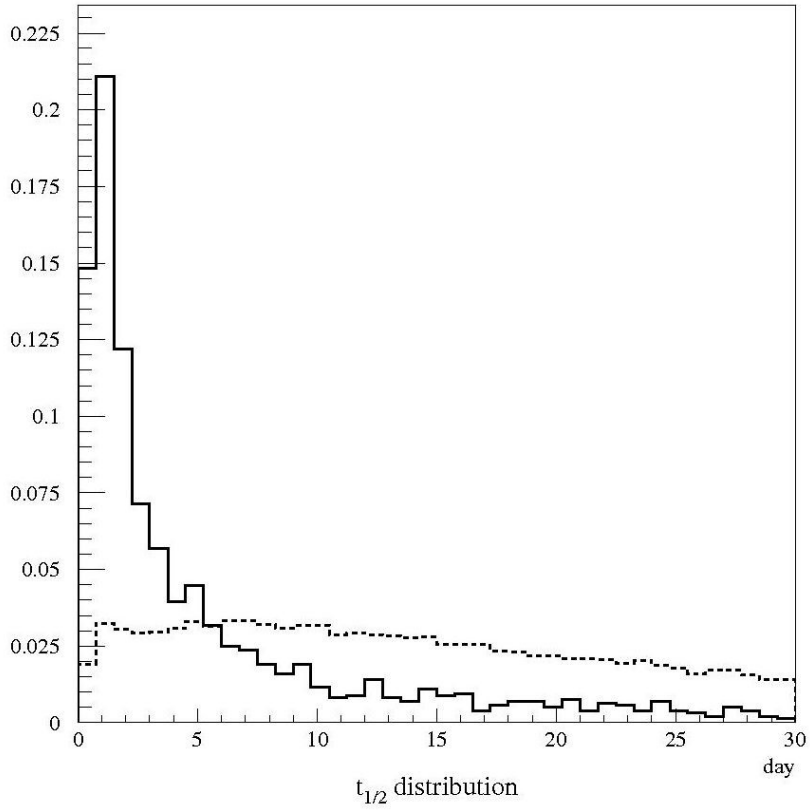

Figure 2. Normalized distributions of $t_{1/2}$ (the duration of a microlensing event without planet) for events with $\chi^2_r > 4$ and $N_{good} > 3$ (solid lines) and for simulated events (dashed lines). Here we take $D = 8$ m telescope parameters.

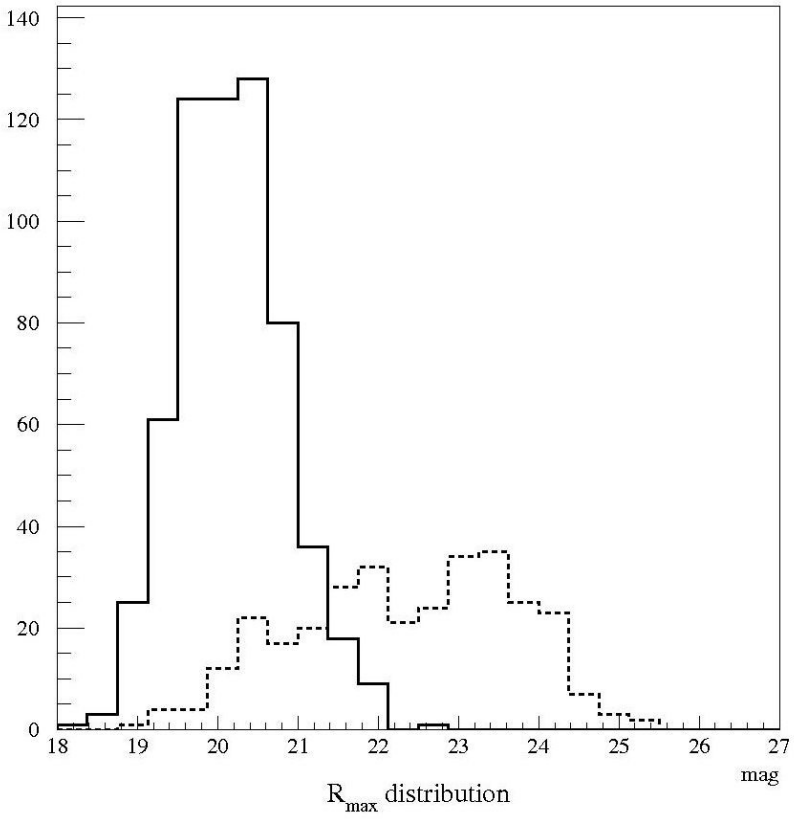

Figure 3. Normalized distributions of R_{max} for events with $\chi^2_r > 4$ and $N_{good} > 3$, assuming a telescope diameter $D = 8$ m. Events with $\rho/u_0 > 1$ (solid line) and $\rho/u_0 < 1$ (dashed line) are shown.

Table 2. Parameters of events shown in Figs. 4 - 8. We also give in the last two columns the sum of residuals χ_r and the maximum value of the mean (with respect to the source area Σ) planetary signal $< \epsilon >_{max}$.

	ρ/u_0	u_0	d_P/R_E	M_P ($M_\oplus$)	θ (deg)	R_E (AU)	t_E (day)	R_{max} (mag)	$t_{1/2}$ (day)	χ_r	$\chi_{r\ max}$	$< \epsilon >_{max}$
#1	2.89	9.47×10^{-3}	0.90	1525	341.8	2.2	16.1	20.2	0.5	194	730	642
#2	1.18	2.63×10^{-2}	0.68	265	104.8	2.8	52.1	21.1	4.0	43	980	249
#3	0.04	3.74×10^{-1}	1.17	0.3	298.0	3.2	23.7	24.1	18.7	9	77	381
#4	0.12	3.56×10^{-1}	2.25	71	190.3	2.3	18.7	23.5	16.5	13	79	566
#5	0.08	1.62×10^{-1}	1.32	1278	336.0	3.9	28.4	23.8	13.3	37	153	1323

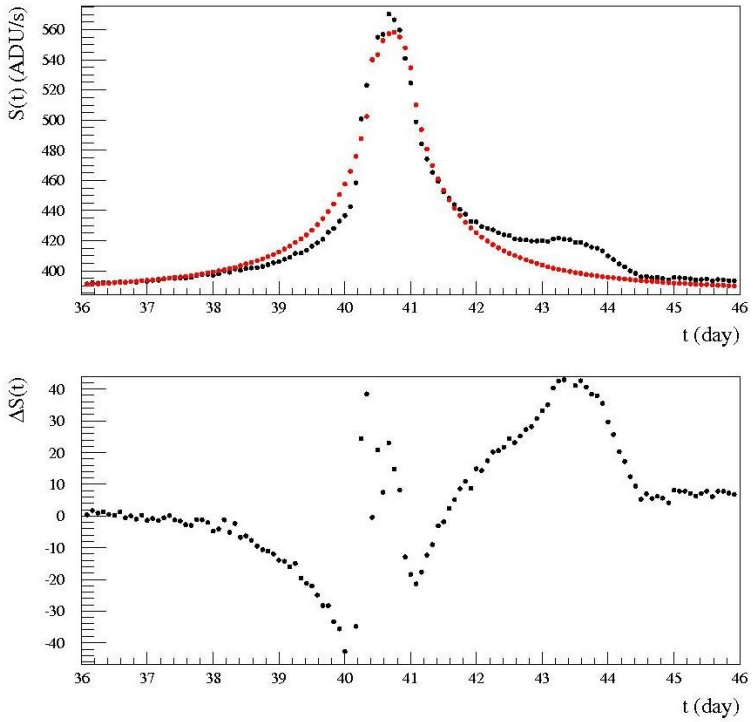

Figure 4. Event of the I class #1 (see Table 2). The upper panel shows the simulated light curve and the corresponding best fit model (a Paczyński light curve modified for finite source effects). The lower panel gives the difference.

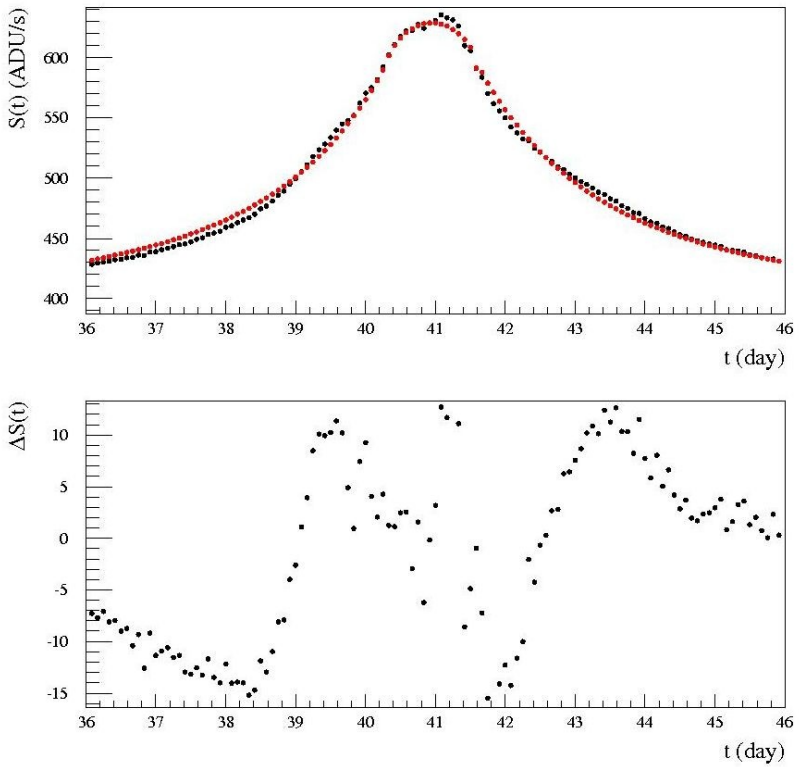

Figure 5. The same as in Fig. 4 for the I class event #2 (see Table 2).

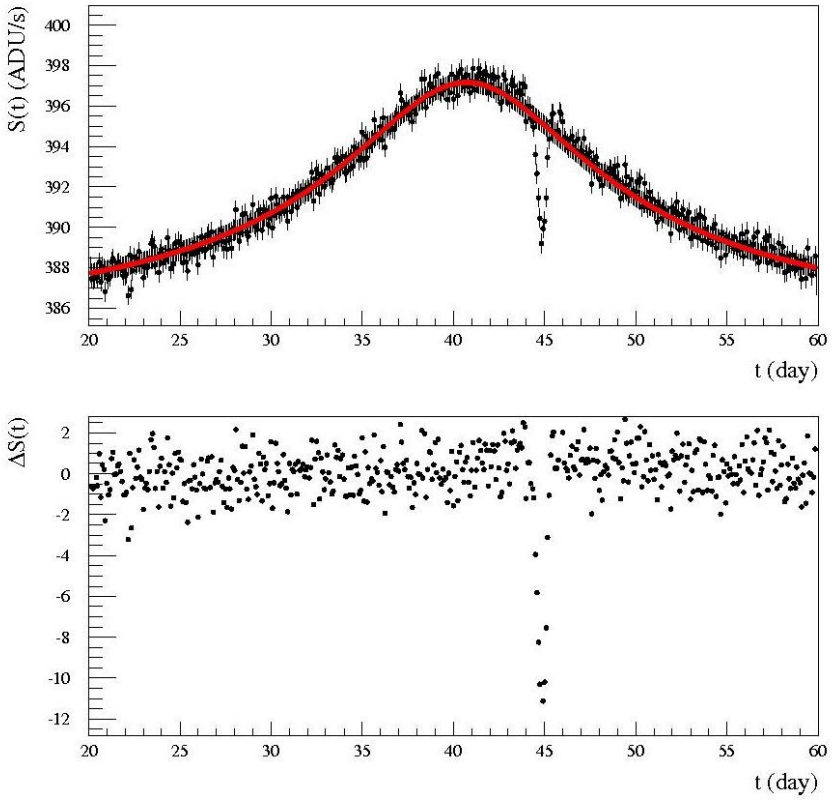

Figure 6. The same as in Fig. 4 for the second class event #3 (see Table 2).

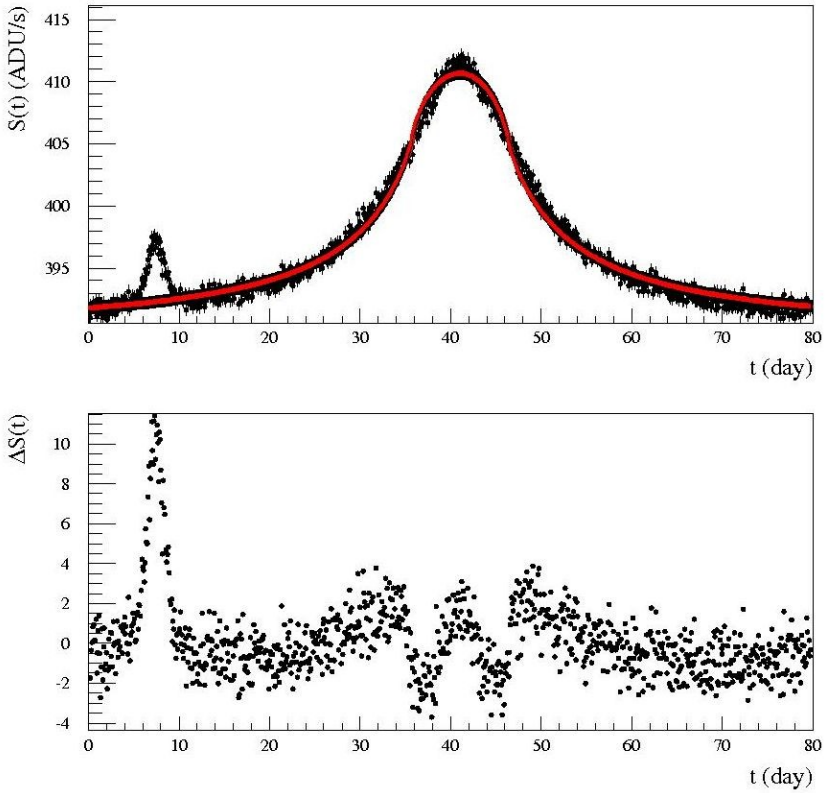

Figure 7. The same as in Fig. 4 for the second class event #4 (see Table 2).

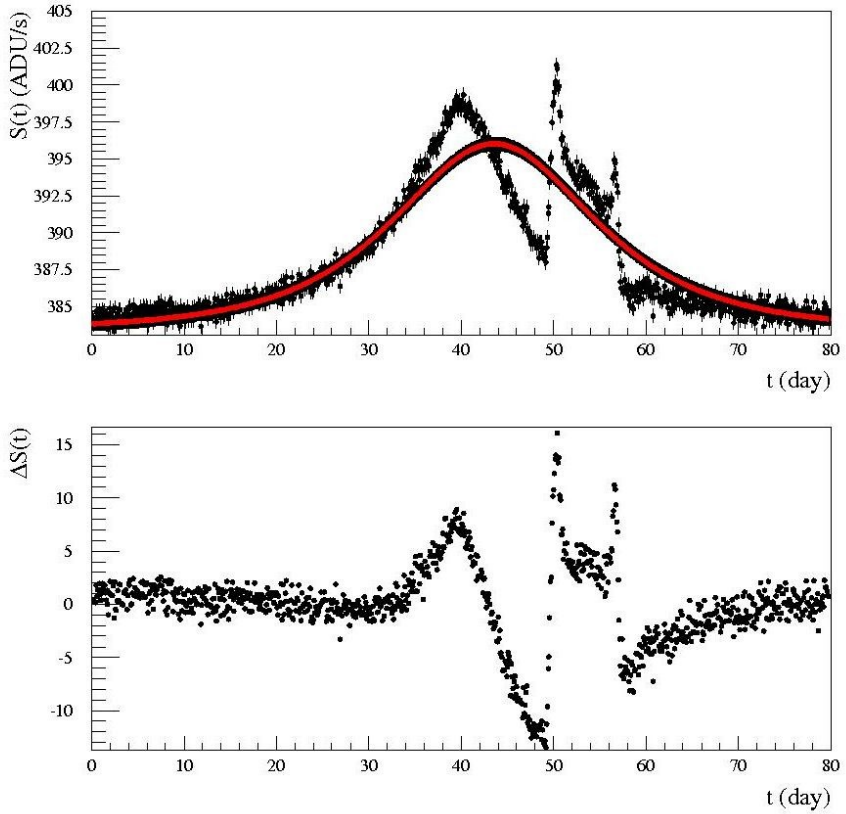

Figure 8. The same as in Fig. 4 for the second class event #5 (see Table 2).

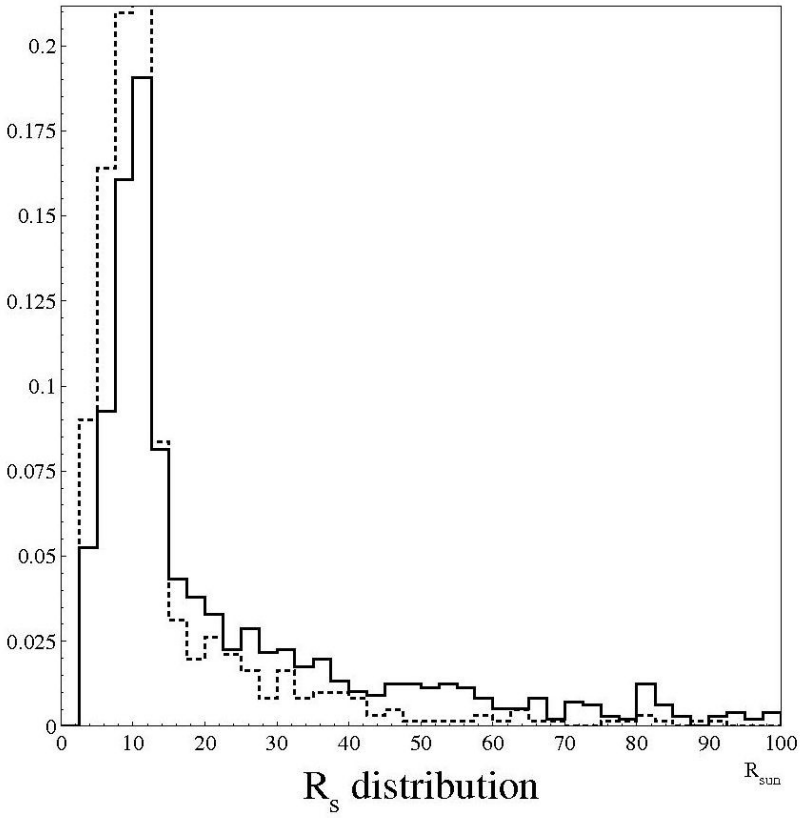

Figure 7. The distribution of the source radius for first (solid line) and second (dashed line) class of events.

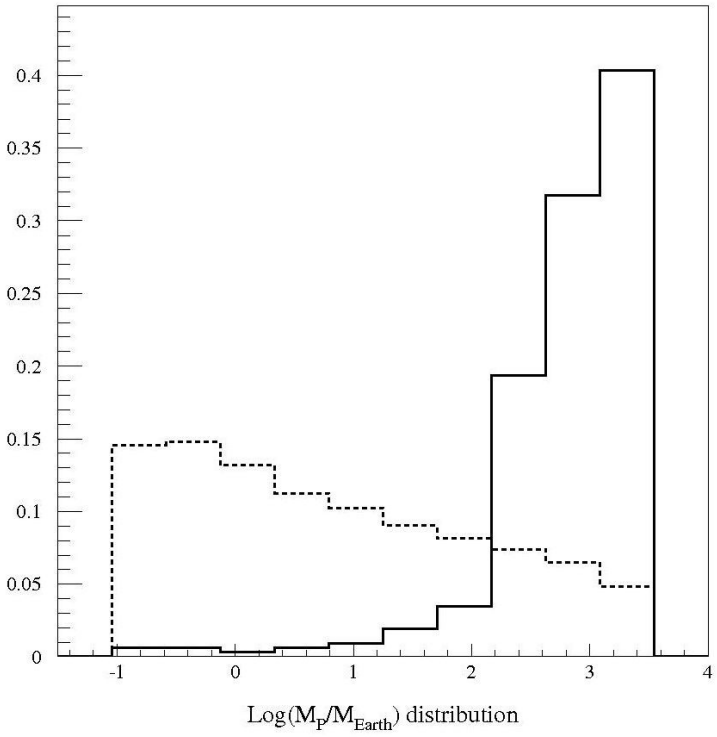

Figure 8. The distribution of the planet mass M_P for the second class of events is shown (solid line). For comparison, the M_P distribution of the generated events is also shown (dashed line). Here we take $N_{im} = 12$ day^{-1} and $D = 8$ m.

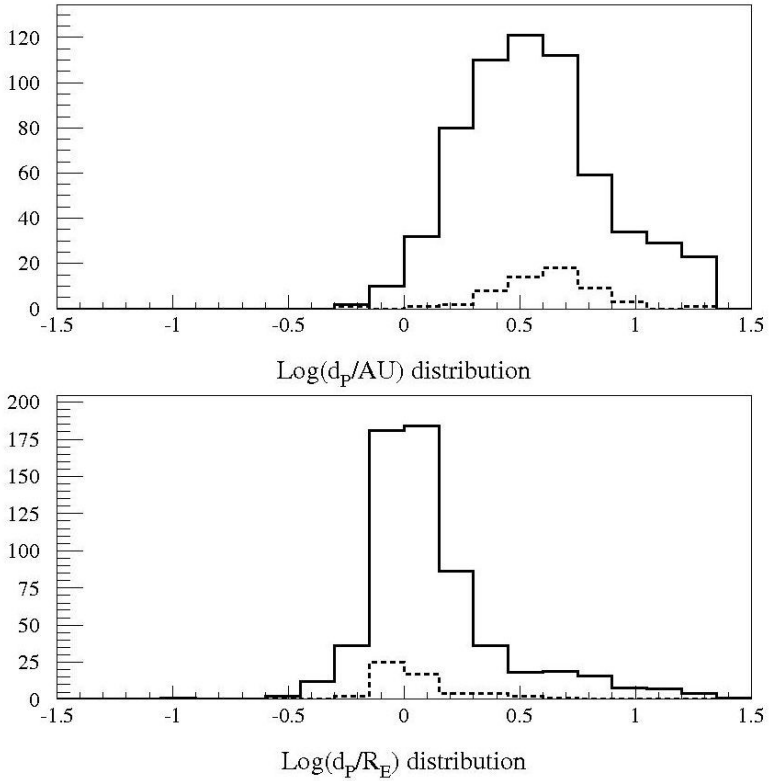

Figure 9. Upper panel: for the second class of events, distributions of the star-to-planet separation d_P (in AU units) for all (solid line) and small planetary mass ($M_P < 20\ M_\oplus$, dashed line). Lower panel: distributions of $s = d_P/R_{\rm E}$ for events as before.

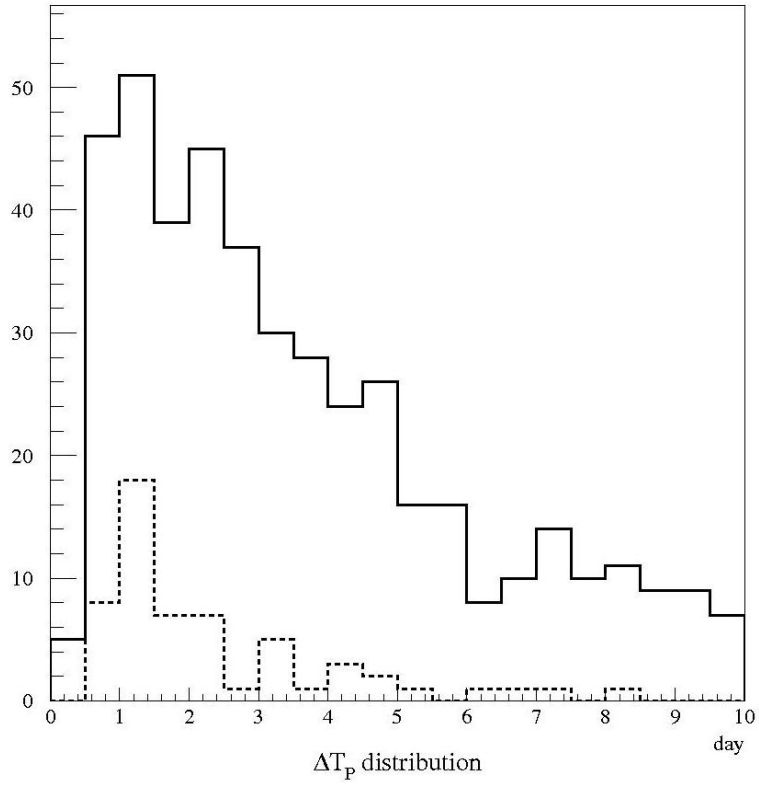

Figure 10. Time duration ΔT_P distributions for all (solid line) and low (dashed line) planetary masses, for the second $(\rho/u_0 < 1)$ class of events.

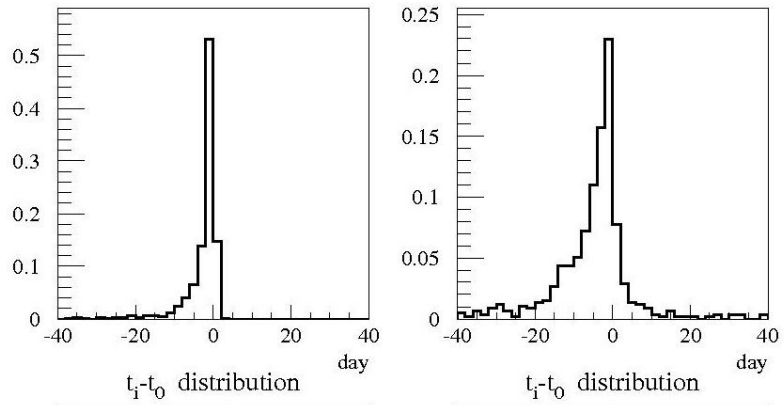

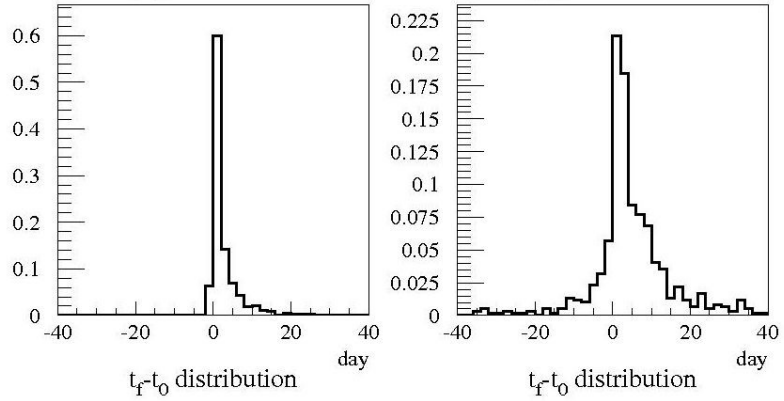

Figure 11. Histograms for the differences $(t_i - t_0)$ (left panels) and $(t_f - t_0)$ (right panels) for first (upper panels) and second (lower panels) classes of events. Initial and final instants for the start and the end of significant (at least 3 points over 3σ) deviations in light curves are denoted by t_i and t_f, while t_0 is the instant of maximum on the light curve for a lens without planet.

Table 1. First class pixel-lensing events ($\chi^2_r > 4$, $N_{good} > 3$ and $\rho/u_0 > 1$). Mean values of lensing parameters: maximum flux deviation $< R_{max} >$, full-width half-maximum event duration $< t_{1/2} >$, Einstein radius $< R_{\rm E} >$, planet-to-star distance $< d_P >$ and planet mass $< M_P >$.

l.o.s.	$< R_s >$ $R_\odot$	$< R_{max} >$ (mag)	$< t_{1/2} >$ (day)	$< R_{\rm E} >$ (AU)	$< d_P >$ (AU)	$< M_P >$ ($M_\oplus$)	$< \Delta T_P >$ (day)
A	26.0	20.01	2.26	2.35	6.34	197	4.3
B	25.2	19.97	2.43	2.73	6.68	148	6.3
C	27.9	19.82	3.14	3.06	6.29	187	7.1
D	24.5	20.18	3.14	2.08	5.99	205	6.3

Table 2. As in Table 1 for the second class pixel-lensing events ($\chi^2_r > 4$, $N_{good} > 3$ and $\rho/u_0 < 1$).

l.o.s.	$< R_s >$ $R_\odot$	$< R_{max} >$ (mag)	$< t_{1/2} >$ (day)	$< R_{\rm E} >$ (AU)	$< d_P >$ (AU)	$< M_P >$ ($M_\oplus$)	$< \Delta T_P >$ (day)
A	14.9	23.31	11.46	2.60	4.99	1024	6.8
B	12.9	22.89	13.12	3.32	4.57	905	9.0
C	14.5	22.94	14.56	3.66	5.68	863	11.3
D	15.1	23.20	13.75	2.50	3.77	929	11.5

Table 3. Probability to detect pixel-lensing events (second column) and to find planetary features ($\chi^2_r > 4$ and $N_{good} > 3$) for first ($\rho/u_0 > 1$, third column) and second ($\rho/u_0 < 1$, fourth column) classes of events for telescopes of different diameters, assuming $N_{im} = 12$ day^{-1} and $t_{exp} = 30$ min.

D (m)	P_{p-l} (%)	P_I (%)	P_{II} (%)
1.5	27	0.1	0.04
2.5	62	0.8	0.46
4	78	1.5	0.78
8	100	2.5	1.53

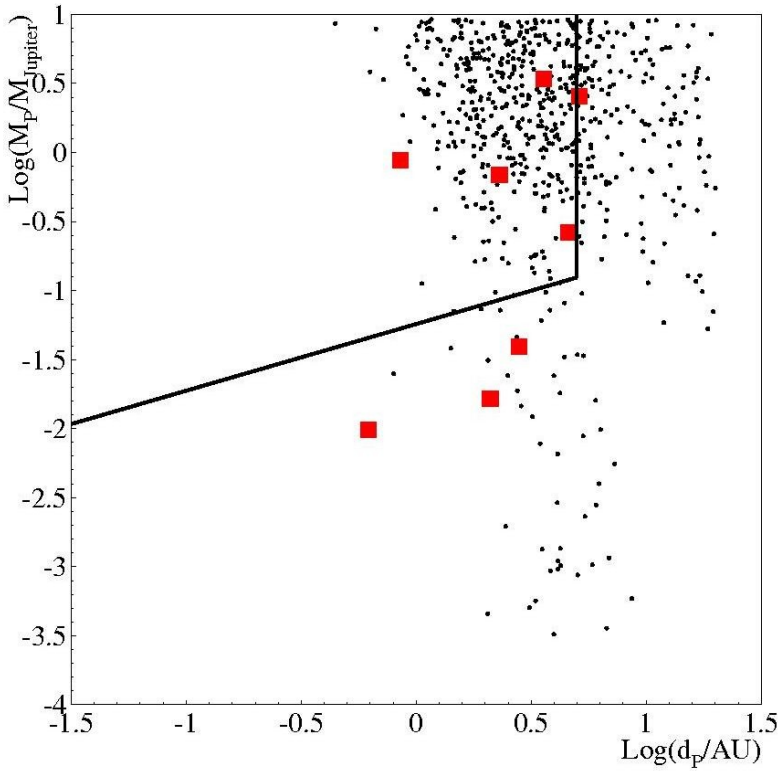

Figure 11. Scatter plot of the planet mass (in unit of Earth mass) vs planet distance (in Astronomical Units). The solid thick line delimits the region (upper and left) of planet detection accessible by the radial velocities, transit and direct imaging methods. The eight small boxes are the planets detected by the microlensing technique. Starting from a sample of 40,000 detectable pixel-lensing events ($D = 8$ m), 630 selected events (indicated by black dots) with $\chi_{\rm r} > 4$, $N_{\rm good} > 3$ and $\langle\epsilon\rangle_{\rm max} > 0.1$ show planetary features and among these 48 events have $M_{\rm P} < 20\ M_{\oplus}$.

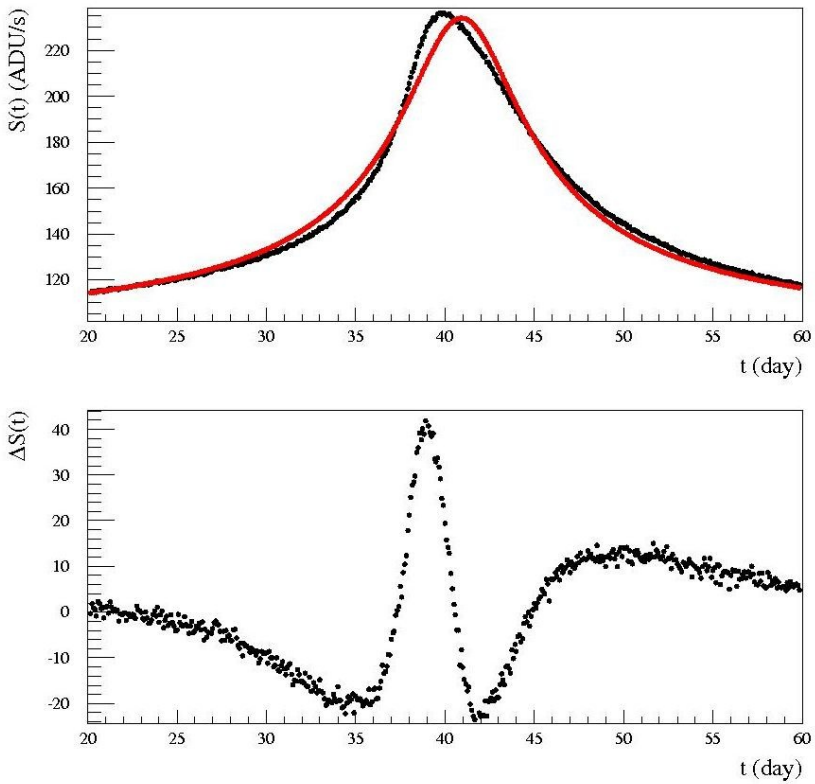

Figure 16. The upper panel shows the simulated light curve of an event with the parameters of the best fit finite source model for the PA-99-N2 event (An et al. 2004). In particular, $d_P = 0.68\ R_E$, $q = 7.59 \times 10^{-3}$ (corresponding to a planet mass $M_P = 2670\ M_\oplus$ for a lens mass of $M_l = 1\ M_\odot$), $u_0 = 0.0386$, $t_E = 124.3$ day, $v_\perp = 340$ km s^{-1} and $\theta = 26.4$ deg. We take the source magnitude $M_r = -2.0$, and a source radius of $R_s = 14\ R_\odot$ (the average radius for a second class event), consistently with the above mentioned analysis. The lower panel gives the difference with respect to the Paczyński light curve (modified for finite source effects) for the same parameters. Here we use the INT telescope parameters and $N_{im} = 12$ day^{-1}.

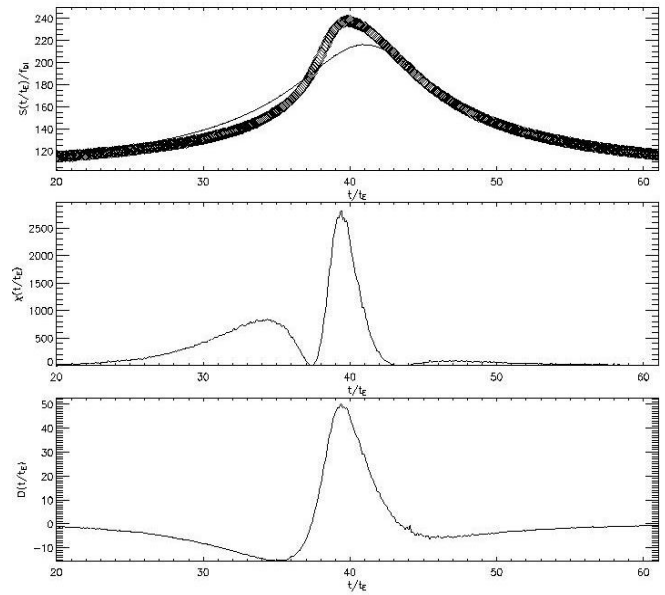

Figure 13. The upper plot shows the simulated light curve of an event with the parameters of the best fit finite source model for the PA-99-N2 event (An et al. 2004). In particular, $d_P = 0.68\ R_E$, $q = 7.59 \times 10^{-3}$ (corresponding to a planet mass $M_P = 2670\ M_\oplus$ for a lens mass of $M_l = 1\ M_\odot$), $u_0 = 0.0386$, $t_E = 124.3$ day, $v_\perp = 340$ km s^{-1} and $\theta = 26.4$ deg. We take the source magnitude $M_r = -2.0$, and a source radius of $R_s = 14\ R_\odot$ (the average radius for a second class event), consistently with the above mentioned analysis. The central plot gives the residuals with respect to the Paczyński light curve (modified for finite source effects) for the same parameters and the lowest plot gives the parameter $\mathcal{D}$. Here we use the INT telescope parameters and $N_{im} = 12$ day^{-1}.

Thanks for your kind attention